University of Alberta

A trial wavefunction approach to the frustrated square-lattice Heisenberg model

by

Xiaoming Zhang

A thesis submitted to the Faculty of Graduate Studies and Research
in partial fulfillment of the requirements for the degree of Master of Science

Department of Physics

Fall 2011
Edmonton, Alberta

To my parents,
Zhenyun Shi and Yuanyu Zhang.

Abstract

Models of interacting quantum spins have contributed significantly to our understanding of magnetism. The Heisenberg model on square lattice, which exhibits semiclassical Néel order, is one of the canonical models. However, with frustration introduced by competing interactions, the system becomes computationally intractable. Exotic quantum phases that have no magnetic long range order may be present due to the frustration. The quantum phases do not have any classical analogue, and a valence bond crystal state with translational and/or rotational symmetry breaking as well as a quantum spin liquid state have been proposed as potential candidates. We construct several trial wavefunctions in the resonating valence bond basis and apply large-scale unbiased calculations to examine the possible descriptions of the ground state in the strongly frustrated region. An analytical master equation is also proposed to provide an approximate solution for the valence bond states. Our numerical and analytical studies suggest that the frustrated ground state exhibits a one-dimensional-like behaviour.

Acknowledgements

I would like to address all the people who stood by my side in my research and thesis writing process with my sincere regards. I owe my deepest gratitude to my supervisor, Dr. Kevin Beach, for his warm encouragement, great efforts in guiding and helping me out of difficulties from the initial to the final stage of my project and careful suggestions on my thesis writing. Without his steadfast support this thesis would not have been possible.

I am heartly thankful to Dr. Andrzej Czarnecki and Dr. Mark Freeman for their valuable feedback towards my research project that helps me improve my method. And I thank all my colleagues for their assistance in my research project, especially Chris Graves for providing his exact diagonalization data on the 4×4 lattice for comparison with my results. As always, I thank my parents for their love and caring for me through my days studying in Edmonton.

Contents

1 Introduction **1**

1.1 Heisenberg model with frustrating interaction 2

1.2 Valence bond basis 4

1.3 Frustration and novel quantum phases 5

2 Simulation algorithms **9**

2.1 Variational Monte Carlo calculation 9

2.1.1 Construct trial wave function 9

2.1.2 Total Energy Evaluation 12

2.1.3 Metropolis algorithm 14

2.1.4 Update 16

2.1.5 Trial State Optimization 17

2.2 Short bond spin liquid calculation 20

2.2.1 Worm algorithm 20

2.3 Measurement of observables 23

3 Numerical and analytical results **25**

3.1 Extending L.D.A. trial wavefunction 26

3.1.1 Unbiased optimization scheme results 26

3.1.2 Master equation for computing bond amplitudes 34
3.1.3 Monte Carlo sampling with master equation results 39
3.1.4 Short bond spin liquid calculation 39
3.2 Symmetry breaking calculation results 42
3.3 Examining bond-bond correlation 50

4 Conclusions **58**

Bibliography **62**

Appendices

A Appendix **65**
A.1 Rewrite the Total Energy into the Form of Weights 65
A.2 Derivation of the Optimization Formula 66

List of Figures

1.1 Possible states with symmetry breaking on a 4×4 lattice 3
1.2 Bipartite and non-bipartite bonds 5
1.3 Different origins of frustration 6
1.4 Checkerboard and collinear AB pattern 7

2.1 Valence bond states overlap with respect to loop structure 11
2.2 Comparison between variational calculation and exact resutls 13
2.3 Basic update step 16
2.4 Change of number of loops 17
2.5 The stochastic optimization scheme is tested on 1D Heisenberg model. 21
2.6 Worm update scheme 22
2.7 A rough qualitative illustration of the phase diagram 24

3.1 Ground state energy from the L.D.A. type trial wavefunction 27
3.2 Energy results from the unbiased optimization (checkerboard) 28
3.3 Order parameters results from unbiased optimization (checkerboard) 29
3.4 Energy results from the unbiased optimization (collinear) 30
3.5 Order parameters results from unbiased optimization (collinear) . . . 31
3.6 Bond amplitudes calculated from unbiased optimization 32
3.7 Bond amplitudes from unbiased calculation 33
3.8 Bond amplitudes from master equation 38
3.9 Sign change 40

3.10 Energy expectation of spin liquid calculation 41
3.11 Comparison of results 41
3.12 Different starting points 43
3.13 Compare energy results (collinear) 44
3.14 Converged unbiased optimization (collinear) 45
3.15 Compare energy results (checkerboard) 46
3.16 Converged unbiased optimization (checkerboard) 47
3.17 Different lattice sizes energy results (checkerboard) 48
3.18 Symmetry breaking calculation results (checkerboard) 49
3.19 Different lattice sizes energy results (collinear) 50
3.20 Symmetry breaking calculation results (collinear) 51
3.21 Measurement M^2 and energy 53
3.22 Staggered magnetization with varying parameter a 55
3.23 C_1 and C_2 values varying with the parameter z 56

CHAPTER 1

Introduction

Models of interacting quantum spins have contributed significantly to the understanding of magnetism. They consist of spin-S objects arranged in a lattice and are meant to describe the behavior of localized electrons in a crystalline environment. The coupling between spins is either ferromagnetic, which favors parallel alignment of spins, or antiferromagnetic (AFM), which favors anti-parallel alignment. The AFM case is the more interesting one since it leads to ground states that are non-classical. When we consider only antiferromagnetic interactions between neighbouring spins on a bipartite lattice, the problem can be easily solved via quantum Monte Carlo approaches [Syljuåsen and Sandvik (2002)] or other numerical methods. Generically, the solution is something close to Néel order. On the square lattice, frustration can be introduced by competing interactions. Exotic quantum phases that have no magnetic long range order may be present due to the frustration. When next-nearest-neighbour interactions are introduced that frustrate the AFM order, the problem becomes computationally intractable. For unbiased studies, the frustration brings on a sign problem that makes Quantum Monte Carlo calculations impossible. Moreover the size of the Hilbert space grows exponentially with system

size and is thus beyond the capability of exact diagonalization (ED) calculations if we want to get near the thermodynamic limit: the largest two-dimensional quantum spin model computed with ED to date is the spin-$\frac{1}{2}$ Heisenberg antiferromagnet on the star lattice with $N = 42$ sites [Richter and Schulenburg (2010); Richter et al. (2004)]. An approximate method such as variational Monte Carlo (VMC) is therefore one of the few remaining possibilities. The study of frustrated spin models is not only important to certain magnetic systems but also gives valuable insight into the behavior of correlated quantum matter, e.g. strongly correlated electrons, localized spins and quantum phase transitions.

1.1 Heisenberg model with frustrating interaction

The Heisenberg hamiltonian including a frustrating interaction has the form

$$H = J_1 \sum_{\langle i,j \rangle} \mathbf{S}_i \cdot \mathbf{S}_j + J_2 \sum_{\langle\langle i,j \rangle\rangle} \mathbf{S}_i \cdot \mathbf{S}_j \tag{1.1}$$

where $J_1 > 0$ and $J_2 > 0$ are the antiferromagnetic exchange couplings. $\langle i, j \rangle$ denotes nearest neighbours corresponding to plaquette edge sites on a square lattice, and $\langle\langle i, j \rangle\rangle$ denotes next nearest neighbors corresponding to sites sitting diagonally across a plaquette. The spin-$\frac{1}{2}$ Heisenberg model on the square lattice has two magnetically ordered ground states for $J_2/J_1 \lesssim 0.4$ and $J_2/J_1 \gtrsim 0.6$ [Dagotto and Moreo (1989); Schulz et al. (1996); Zhitomirsky and Ueda (1996); Sushkov et al. (2001); Capriotti et al. (2003); Bishop et al. (1998); Beach (2009)]. The former is the well known Néel ordered state with antiparallel spins on nearest neighbour sites. The latter system can be seen as two interpenetrating square-lattice Heisenberg antiferromagnets rotated 45° with respect to the original lattice. At exactly $J_2/J_1 = \infty$,

the two subsystems are uncoupled. Collinear order emerges when $J_1 > 0$; the two antiferromagnets lock to each other since the relative direction of the antiferromagnetic order in spin space between the two subsystems is no longer arbitrary [Sandvik (2010)]. The physics of the phase in the intermediate region is not yet clear, but it is believed to be short-ranged and not to exhibit any kind of classical magnetic order. A state with broken translational symmetry (see Fig. 1.1) is one possibility: a valence bond crystal with plaquette order [Capriotti and Sorella (2000)], which is a spontaneous dimerization with broken translation symmetry but with rotation symmetry still retained; or a valence bond crystal with columnar order, which spontaneously breaks both rotational and translational symmetry [Dagotto and Moreo (1989)]. A featureless spin liquid that doesn't break any symmetries was also proposed as a possible ground state [Capriotti et al. (2001); Anderson (1987)].

(a) Columnar order (b) Plaquette order

Figure 1.1: Possible states with symmetry breaking on a 4×4 lattice

1.2 Valence bond basis

To study the frustrated Heisenberg model, we can make use of the valence bond (VB) basis in numerical calculations instead of the usual basis of S^z eigenstates. This has benefits in terms of both qualitative insights and computational utility [Lou and Sandvik (2007)]. A valence bond (i, j) denotes a pair of oppositely directed spins at sites i and j that form a singlet: $(i, j) = (|\uparrow_i\downarrow_j\rangle - |\downarrow_i\uparrow_j\rangle)/\sqrt{2}$. In a system of $S = \frac{1}{2}$ spins numbering N, each valence bond state consists of $N/2$ singlet pairs. In contrast with the S^z basis, the valence bond basis is nonorthogonal and overcomplete. We can expand any total singlet state as a sum of states that are products of valence bonds [Sandvik (2005)]:

$$|\Psi\rangle = \sum_\alpha f_\alpha |(a_1^\alpha, b_1^\alpha)\cdots(a_{N/2}^\alpha, b_{N/2}^\alpha)\rangle = \sum_\alpha f_\alpha |V_\alpha\rangle, \tag{1.2}$$

where $(a, b) = (|\uparrow_a\downarrow_b\rangle - |\downarrow_a\uparrow_b\rangle)/\sqrt{2}$.

We can obtain a more restricted but still overcomplete basis by dividing the sites into two groups, A and B, which typically correspond to the two sublattices in a bipartite lattice. A valence bond can only be formed between two sites from different groups (bipartite bond, see Fig. 1.2(a)).

The overcompleteness property holds as $(i, k)(j, l) = (i, j)(k, l) - (i, l)(k, j)$. Thus the non-bipartite bonds can be eliminated through the overcompleteness property. And the bond by convention has direction as $(i, j) = -(j, i)$, indicating the order of spins in the singlet definition.

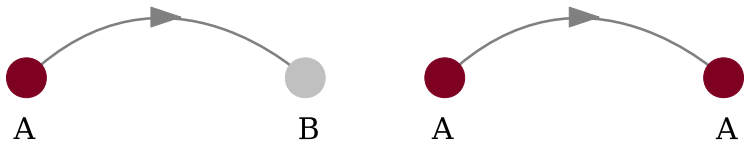

(a) Bipartite bond (b) Non-bipartite bond

Figure 1.2: (a) The bipartite bond is formed between different sublattices. (b) The non-bipartite bond connects sites in the same sublattice.

1.3 Frustration and novel quantum phases

Frustration in our context describes the situation where competing antiferromagnetic exchange interactions can not be fulfilled at the same time [Balents (2010)]. The frustration may be geometric in origin, e.g. on triangle-like lattices where the three spins on vertices can not be antiparallel aligned simultaneously (see Fig. 1.3(a)), or it may come about due to competing interactions, as in the square-lattice model with nearest- and next-nearest AFM exchange (see Fig. 1.3(b)).

Without frustration, the ground state of the Heisenberg hamiltonian on a square-lattice exhibits a semiclassical Néel order. Whereas with competing interaction added in, the long range magnetic order is disrupted in the intermediate phase region. A quantum phase without any classical analogue emerges, which means we can not fully detect this by order parameters based on a magnetic structure factor.

One significant property greatly affected by frustration is the manifestation of the Marshall's sign rule. The Marshall's sign rule holds for Heisenberg hamiltonian with antiferromagnetic exchange couplings J_{ij} between two different sublattices A and B on a bipartite lattice; the ground state $|\Psi_{GS}\rangle$ can be chosen to have an expansion

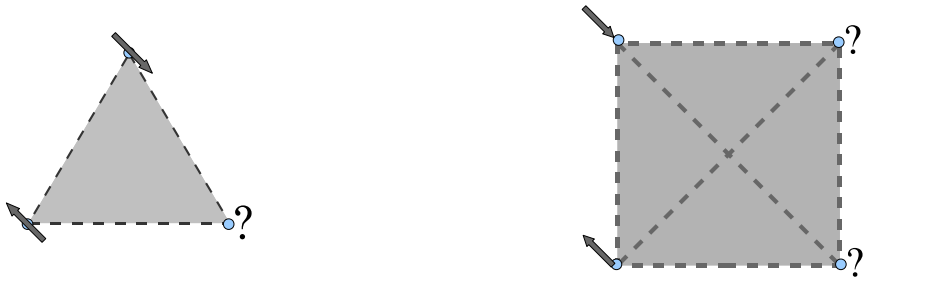

(a) Frustration on the triangular lattice (b) Frustration on the square lattice

Figure 1.3: Frustration can have different origins, for example, geometric frustration on triangular lattices, or frustration due to next nearest neighbour interactions on square lattices.

$|\Psi_{GS}\rangle = \sum_\alpha f_\alpha |\phi_\alpha\rangle$ with a predictable $\pm$ sign of each coefficient in an Ising basis where $|\phi_\alpha\rangle$ has a form of $|\uparrow\downarrow\uparrow\uparrow\downarrow\downarrow\rangle$ [Marshall (1955); Lieb et al. (1961)]. In the language of the valence bond basis, obeying the Marshall sign rule means that each coefficient f_α of the valence bond state $|V_\alpha\rangle$ is positive definite, which is extremely important for large scale unbiased calculations such as Monte Carlo methods since it is directly related to the sign problem. In Monte Carlo sampling, the coefficient of each valence bond state determines its probability. When a frustrating interaction exists between sites in the same sublattice, the Marshall's sign rule will gradually break down. The negative coefficient will lead to negative probability while we can only sample with positive probability in Monte Carlo calculations: In a fermionic quantum system an observable $\hat{O}$ is measured as

$$\langle \hat{O} \rangle = \frac{\mathrm{Tr}[\hat{O}\exp(-\beta H)]}{\mathrm{Tr}[\exp(-\beta H)]} = \frac{\sum_i O_i p_i}{\sum_i p_i} \tag{1.3}$$

whenever negative p_i emerges, the sampling process will become impossible due to

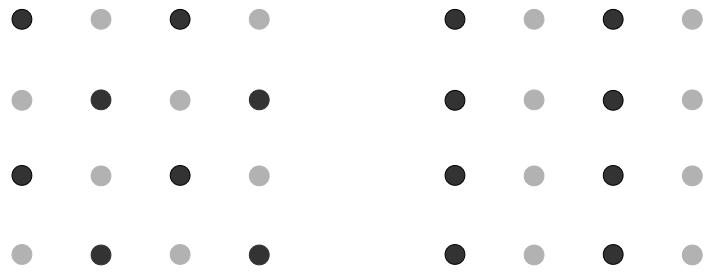

(a) Checkerboard AB pattern (b) Collinear AB pattern

Figure 1.4: We can assign AB labels on square lattice in different ways. We work on checkerboard AB pattern and collinear AB pattern. The dots shown in dark or light grey colour denote different groups of sites.

the sign problem. It is possible to sample instead with respect to the absolute value of the probability and to absorb the sign into a measurement in the numerator and denominator

$$\langle \hat{O} \rangle = \frac{\sum_i O p_i}{\sum_i p_i} = \frac{\sum_i \mathrm{sign}_i |p_i| \hat{O} / \sum_i |p_i|}{\sum_i \mathrm{sign}_i |p_i| / \sum_i |p_i|} \equiv \frac{\langle \mathrm{sign} \cdot \hat{O} \rangle_{|p|}}{\langle \mathrm{sign} \rangle_{|p|}}, \tag{1.4}$$

The error grows exponentially, however, and the sampling process becomes unreliable. Thus this can only be applied to systems with a slight sign problem. Typically the denominator $\langle \mathrm{sign} \rangle_{|p|} \sim e^{-(const.) \times L^d}$ where d is the dimension of the system, so this only works for small lattices.

For this work, the Marshall's sign rule depends on which AB pattern (checkerboard or collinear) we choose in constructing our basis (see Fig. 1.4(a), 1.4(b)). That pattern is not necessarily coincident with the sublattice structure of the underlying lattice.

Our work involves a basis choice. We do not construct the trial wave functions from the largest possible set of valence bond states in which all spins are joined in all

possible ways. Instead we obtain a more restricted basis by dividing the system into two groups of sites (A and B) and only keeping states in which bonds connect A sites and B sites (bipartite bonds). No approximation is involved in this process since the restricted basis is so massively overcomplete that even in this subset still spans the relevant part of the Hilbert space.

In assigning A and B labels to the sites, we are making choices about the form of the trial wavefunction for the reason that bond amplitudes h_{ij} are fixed to be positive definite. By working with the checkerboard AB pattern on the left and with the collinear AB pattern on the right, we are in essence adapting the trial wavefunction to $J_2/J_1 = 0$ and $J_2/J_1 = \infty$ and taking advantage of the Marshall's sign rules that exist in the two limits. However we are not biasing the wavefunction in the sense that we are "building in" any kind of magnetic order. The wavefunctions constructed from either AB pattern are fully capable of representing non-magnetic states.

CHAPTER 2

Simulation algorithms

2.1 Variational Monte Carlo calculation

2.1.1 Construct trial wave function

For a finite bipartite lattice, the ground state of the Heisenberg model is a total singlet state and obeys Marshall's sign rule. With this condition, Fazekas and Anderson [Fazekas and Anderson (1974); Anderson (1973)] proposed a particularly useful set of variational states, *Resonating Valence Bond* (RVB) states for the spin-$\frac{1}{2}$ antiferromagnetic Heisenberg model. Consider singlet eigenstates of the Heisenberg model on bipartite lattice, which can be expanded in valence bond states

$$|\Psi\rangle = \sum_{\alpha} f_{\alpha} |(a_1^{\alpha}, b_1^{\alpha}) \cdots (a_{N/2}^{\alpha}, b_{N/2}^{\alpha})\rangle = \sum_{\alpha} f_{\alpha} |V_{\alpha}\rangle, \tag{2.1}$$

where

$$|V_{\alpha}\rangle = \prod_{(i,j)\in V_{\alpha}}^{i\in A, j\in B} \frac{1}{\sqrt{2}} (|\uparrow_i \downarrow_j\rangle - |\downarrow_i \uparrow_j\rangle) \tag{2.2}$$

The coefficients f_α can be approximated by products of amplitudes h_{ij} that are taken to be real and positive:

$$f_\alpha = \prod_{i\in A, j\in B} h_{ij}. \tag{2.3}$$

This amplitude product form is straightforward to optimize, with the bond amplitudes h_{ij} serving as variational parameters. Except in a few special cases, we can not evaluate the correlations of valence bond states analytically because it involves summing over an exponentially large number of contributions. For an N-site square lattice, the number of coefficients f_α is $(N/2)!$, and the product amplitude ansatz leads to $(N/2)^2$ variational parameters. Still, even $O(N^2)$ is too expensive to carry out with the increasing of lattice size. However, we can greatly reduce the complexity of this problem by taking advantage of the symmetry property. For example, we might treat the bond amplitudes as translationally invariant; thus they can take the form $h_{ij} = h(\mathbf{r}_{ij})$ where $\mathbf{r}_{ij} = \mathbf{r}_i - \mathbf{r}_j$. The size of the set of variational parameters is thus reduced to $O(N)$. In their VMC study, Liang, Douçot and Anderson [Liang et al. (1988)] further reduced the number of variational parameters to one by imposing a functional form for the amplitudes $h(r)$ — decaying as $h_{ij} = |\mathbf{r_i} - \mathbf{r_j}|^{-p}$ where i and j are bond endpoints. This trial wave function can describe almost perfectly the long range Néel order of the ground state of the Heisenberg model at $J_2 = 0$. The bond amplitudes h_{ij}, understood as variational parameters, are adjustable in the minimization of the expectation value of ground state energy. Through the sampling of bond configurations, the amplitude product state can be studied and the RVB states can be used as variational states for both ordered and disordered phases [Sandvik (2010)].

In our calculation, the model is built on $L \times L$ square-lattice model. Periodic

boundary conditions are applied so that each lattice site has the same geometric surroundings and thus are all equivalent and the whole lattice is translationally invariant. Edge spins that would cause different properties are avoided, which can help to make the calculation reliable. For an $L \times L$ lattice with these boundary conditions, the valence bond has Manhattan length ranging from 1 to $L-1$.

In the Monte Carlo calculation, the observable expectation values are obtained as an ensemble average of an estimator $\frac{\langle V_{\alpha'}|\hat{O}|V_\alpha\rangle}{\langle V_{\alpha'}|V_\alpha\rangle}$ [Beach and Sandvik (2006)]:

$$\langle \hat{O} \rangle = \left\langle \frac{\langle V_{\alpha'}|\hat{O}|V_\alpha\rangle}{\langle V_{\alpha'}|V_\alpha\rangle} \right\rangle_w = \frac{\sum_{\alpha'\alpha} W_{\alpha'} W_\alpha \frac{\langle V_{\alpha'}|\hat{O}|V_\alpha\rangle}{\langle V_{\alpha'}|V_\alpha\rangle}}{\sum_{\alpha'\alpha} W_{\alpha'} W_\alpha} \tag{2.4}$$

sampled with the weight

$$W_{\alpha'} W_\alpha = \langle V_{\alpha'}|V_\alpha\rangle f^*_{\alpha'} f_\alpha = 2^{N_l - \frac{N}{2}} \prod_{\mathbf{r}_{ij} \in V_{\alpha'}, V_\alpha} h(\mathbf{r}_{ij})^{n(\mathbf{r}_{ij})}. \tag{2.5}$$

Here N_l is the number of loops and N is the total number of spins. $2^{N_l - \frac{N}{2}}$ is an expression for the overlap between two VB states (see fig2.1(c)).

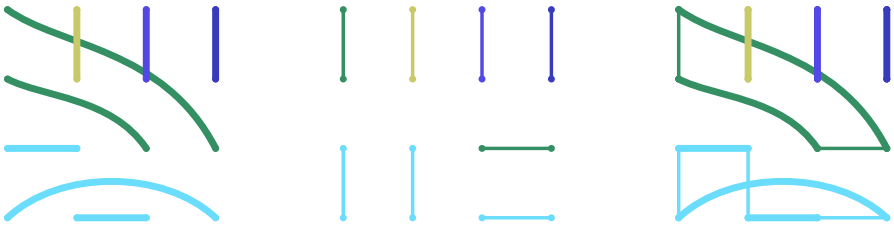

(a) $\langle V_{\alpha'}|$ (b) $|V_\alpha\rangle$ (c) $\langle V_{\alpha'}|V_\alpha\rangle$

Figure 2.1: Valence bond states overlap with respect to loop structure: Each of $\langle V_{\alpha'}|V_{\alpha'}\rangle$ and $\langle V_\alpha|V_\alpha\rangle$, since there are no bond mismatches, give rise to eight short loops. On the other hand $\langle V_{\alpha'}|V_\alpha\rangle$ has five loops.

Liang et al. had shown that the ground state of the two-dimensional Heisenberg model with nearest neighbour interactions, which has a Néel ordered ground state, requires an algebraic decay of the bond length probability [Liang et al. (1988)]. The decaying form $h(r)$ they proposed however did not describe how the amplitudes change when competing interactions such as next nearest neighbour interactions are introduced. The power law form of bond amplitude leads to isotropic bonds since it only decays with bond length. It does not allow symmetry breaking and can well describe a spin liquid state which retains lattice symmetry. Therefore it is impossible to achieve any candidate states with symmetry breaking proposed as the ground state for the intermediate phase of the $J_1 - J_2$ model with a next nearest neighbor interaction added as $H = \sum_{\langle i,j\rangle} J_1 \mathbf{S}_i \cdot \mathbf{S}_j + \sum_{\langle\langle i,j\rangle\rangle} J_2 \mathbf{S}_i \cdot \mathbf{S}_j$. This trial wave function works well for nonfrustrating interactions, but when $J_2 \neq 0$ it fails, with the antiferromagnetism gradually killed by increasing frustration near $J_2/J_1 = 0.4$ (see fig 2.2).

2.1.2 Total Energy Evaluation

The energy of the trial wave function can be written as a weighted sum, i.e. the expectation value of energy of the system:

$$E = \langle\psi|H|\psi\rangle = \frac{\sum_L W(\mathcal{L})E(\mathcal{L})}{\sum_{\mathcal{L}} W(\mathcal{L})}, \tag{2.6}$$

where $\mathcal{L} = (V_{\alpha'}, V_\alpha)$ refers to loop structure (detailed derivation can be found in Appendix A.1). The weight of each loop configuration is

$$W(\mathcal{L}) = \langle V_{\alpha'}|V_\alpha\rangle f^*_{\alpha'} f_\alpha = 2^{N_l - \frac{N}{2}} \prod_{i\in A, j\in B} h(\mathbf{r}_{ij})^{n(\mathbf{r}_{ij})}. \tag{2.7}$$

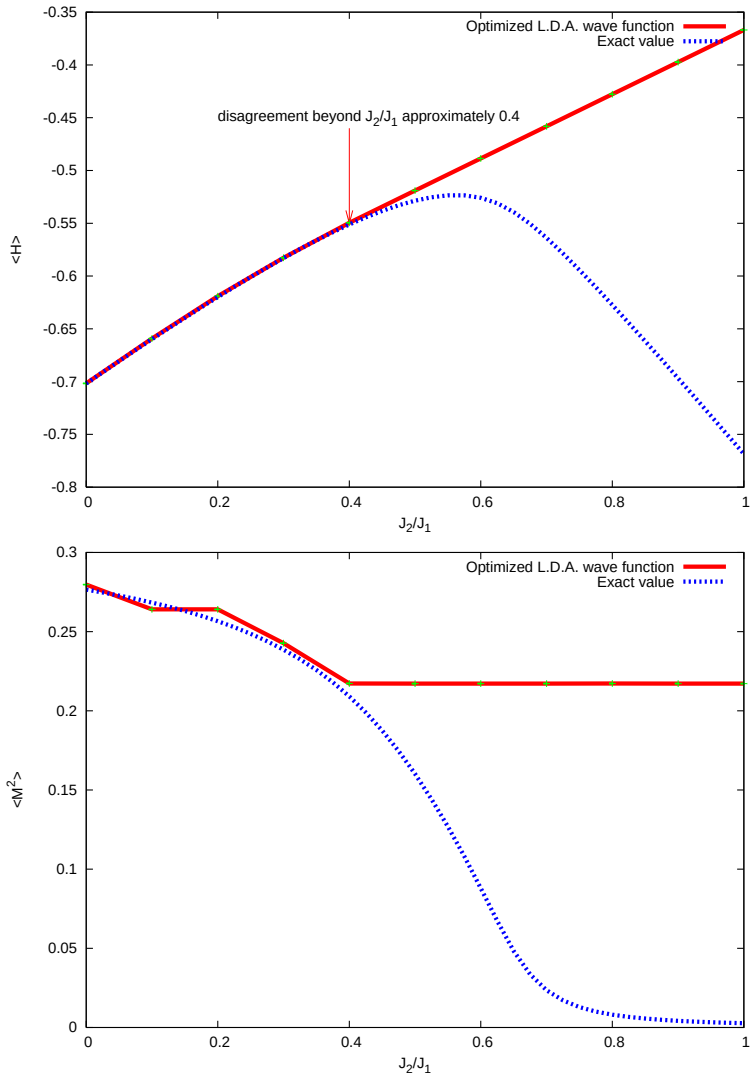

Figure 2.2: Comparision between results of variational calculation with L. D. A. trial wave function and exact results on 4×4 lattice

For these wave functions the calculation of expectation values for the energy and the spin-spin correlation functions can be implemented with only a few simple rules. In order to calculate overlaps between two valence bond configurations $|V_\alpha\rangle$ and $|V_{\alpha'}\rangle$, and matrix elements of $\mathbf{S}_i \cdot \mathbf{S}_j$ between those states, we need first to consider the loop covering of the plane associated to the configurations $|V_\alpha\rangle$ and $|V_{\alpha'}\rangle$ (see Fig. 2.1(c)).

For a bipartite system, the overlap of two VB states is determined by the loops formed when bonds are superimposed, as illustrated in Fig. 2.1(c). Each loop has two compatible spin states and the overlap follows $\langle V_{\alpha'}|V_\alpha\rangle = 2^{N_{loop}-\frac{N}{2}}$ which replaces the standard overlap for an orthogonal basis $\langle\psi_{\alpha'}|\psi_\alpha\rangle = \delta_{\alpha'\alpha}$. Fig. 2.1(c) shows two VB states in two dimensions and their overlap in terms of loops formed by superimposing the two bond configurations. In this case, there are $N_v = 8$ valence bonds and $N_l = 4$ loops, and $\langle V_{\alpha'}|V_\alpha\rangle = 2^{N_{loop}-\frac{N}{2}} = 1$. Matrix elements $\frac{\langle V_{\alpha'}|\mathbf{S}_i\cdot\mathbf{S}_j|V_\alpha\rangle}{\langle V_{\alpha'}|V_\alpha\rangle}$ are also easily obtained from these loops:

$$\frac{\langle V_{\alpha'}|\mathbf{S}_i \cdot \mathbf{S}_j|V_\alpha\rangle}{\langle V_{\alpha'}|V_\alpha\rangle} = \begin{cases} +\frac{3}{4} & \text{if } i \text{ and } j \text{ belong to the same loop, + for the same sublattice} \\ -\frac{3}{4} & \text{if } i \text{ and } j \text{ belong to the same loop, − for different sublattices} \\ 0 & \text{if } i \text{ and } j \text{ belong to two different loops} \end{cases} \tag{2.8}$$

2.1.3 Metropolis algorithm

Because the number of terms in the sum (see Eqn. 2.6) grows exponentially with the size of the system, the phase space to be summed over can be considered as an

ensemble of pairs $\mathcal{L} = (V_{\alpha'}, V_\alpha)$ with a probability distribution

$$P(\mathcal{L}) = \frac{W(\mathcal{L})}{\sum W(\mathcal{L})}. \tag{2.9}$$

This interpretation is valid because the $P(\mathcal{L})$ is always positive. For a given set of amplitudes h, we evaluate the energy using the Metropolis Monte Carlo algorithm. The basic Monte Carlo update step of the bond configuration is to choose two next nearest-neighbour sites i, i_2 (or in principle any i, i_2 in the same sublattice, but the acceptance rate decreases with increasing distance between the sites), and reconfigure bonds $(i,j)(i_2,k)$ to which they are connected, according to $(i,j)(i_2,k) \longrightarrow (i,k)(i_2,j)$ where the labels here correspond to both sites i and i_2 being in sublattice A. As there are only two bonds involved in each update step, we do not need to calculate the ratio of the full weight; the Metropolis acceptance Probability P for such a update from state $\mathcal{L}$ to state $\mathcal{L}'$ is very easy to calculate in terms of amplitude ratios and the change in the number of loops, ΔN_l, which is determined by the change of loop structure due to bond reconfiguration,

$$P_{\mathcal{L}\to\mathcal{L}'} = \min\left[\frac{h(\mathbf{r}_{ik})h(\mathbf{r}_{i_2j})}{h(\mathbf{r}_{ij})h(\mathbf{r}_{i_2k})} 2^{\Delta N_l}, 1\right]. \tag{2.10}$$

It satisfies the detailed balance condition that

$$P_{\mathcal{L}} W(\mathcal{L}\to\mathcal{L}') = P_{\mathcal{L}'} W(\mathcal{L}'\to\mathcal{L}). \tag{2.11}$$

If $P_{\mathcal{L}\to\mathcal{L}'} = 1$, the bond reconfiguration is accepted. If not, a random number $R \in [0,1)$ will be generated and compared to $P_{\mathcal{L}\to\mathcal{L}'}$. If $P_{\mathcal{L}\to\mathcal{L}'} > R$, the update will be accepted; otherwise, it will be rejected. For the two dimensional simulation, the update step is to randomly choose one site (i,j) and then choose one of its four

diagonal neighbor sites i_2 randomly, exchange the ends of the bonds $(i,j)(i_2,k) \longrightarrow (i,k)(i_2,j)$. The reason for choosing two sites from the same sublattice is that only in this way can we avoid forming non-bipartite bonds through bond reconfiguration.

2.1.4 Update

The update move is to swap the bond endpoints at j and k as illustrated in Fig. 2.3. In one dimension the swap is taken place between site i and next nearest neighbor site i_2 and for two dimensional system it is between site i and one of its diagonal neighbor sites. There are three types of updates; take the two dimensional case for example, for bonds (i,j) and (i_2,k) the updates can be

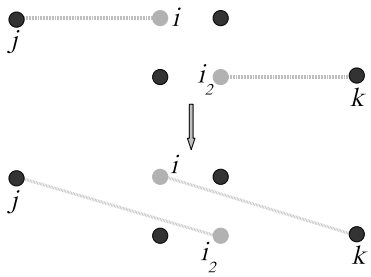

Figure 2.3: Basic update step

2 loops join into 1 (see Fig. 2.4(a)), the corresponding weight is

$$\delta = \frac{2^1 h(\mathbf{r}_{ik}) h(\mathbf{r}_{i_2 j})}{2^2 h(\mathbf{r}_{ij}) h(\mathbf{r}_{i_2 k})} = \frac{h(\mathbf{r}_{ik}) h(\mathbf{r}_{i_2 j})}{2 h(\mathbf{r}_{ij}) h(\mathbf{r}_{i_2 k})} \tag{2.12}$$

loop number is preserved, the corresponding weight is

$$\delta = \frac{2^1 h(\mathbf{r}_{ik}) h(\mathbf{r}_{i_2 j})}{2^1 h(\mathbf{r}_{ij}) h(\mathbf{r}_{i_2 k})} = \frac{h(\mathbf{r}_{ik}) h(\mathbf{r}_{i_2 j})}{h(\mathbf{r}_{ij}) h(\mathbf{r}_{i_2 k})} \tag{2.13}$$

or *1 loop splits into 2* (see Fig. 2.4(b)), the corresponding weight is

$$\delta = \frac{2^2 h(\mathbf{r}_{ik}) h(\mathbf{r}_{i_2 j})}{2^1 h(\mathbf{r}_{ij}) h(\mathbf{r}_{i_2 k})} = \frac{2 h(\mathbf{r}_{ik}) h(\mathbf{r}_{i_2 j})}{h(\mathbf{r}_{ij}) h(\mathbf{r}_{i_2 k})}. \tag{2.14}$$

The probability is obtained as $\min(\delta, 1)$ and is compared with the random number $R \in [0, 1)$. The update will be accepted if $\min(\delta, 1) > R$ and otherwise rejected.

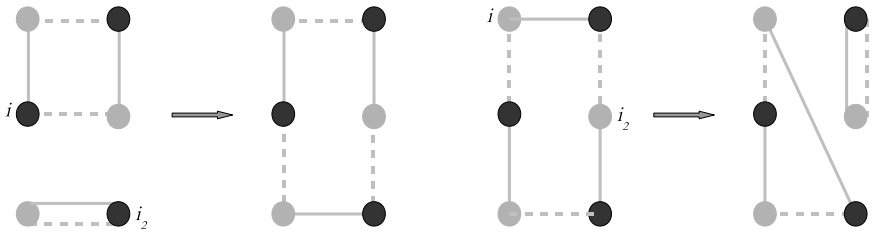

(a) Two loops join into 1 (b) One loop splits into 2

Figure 2.4: Change of number of loops

Tests are carried out to verify the data structures after each update. The number of loops, the distance (i.e. the bond length), and for each singlet whether the corresponding relation is maintained are checked after every update step.

The system should be thermalized before the optimization and measurement process. Within our program, thermalization is judged according to whether the fluctuation of total energy is small enough.

2.1.5 Trial State Optimization

With the correction term, a set of parameters for the trial wave function of entangled pairs can be introduced. For each J_2/J_1, the corresponding set of parameters can be optimized to find the $\langle H \rangle$ minimum. For the quantum Hamiltonian $\hat{H}$ with

eigenstates $\hat{H}|\psi_n\rangle = E_n|\psi_n\rangle$, the true ground state $|\psi_0\rangle$ has energy E_0. And as stated before, any trial state $|\psi\rangle$ will have an energy expectation value

$$E = \frac{\langle\psi|H|\psi\rangle}{\langle\psi|\psi\rangle} \geq E_0. \tag{2.15}$$

The family of trial states is parameterized by $\vec{x} = (x_1, x_2, \cdots, x_N)$, the corresponding energy landscape is $E(\vec{x})$. We improve energy locally by moving *downhill*, i.e. along

$$-\vec{\nabla}E = -(\frac{\partial E}{\partial x_1}, \frac{\partial E}{\partial x_2}, \cdots, \frac{\partial E}{\partial x_N}), \tag{2.16}$$

and use stochastic optimization initially proposed by Lou and Sandvik [Lou and Sandvik (2007)], where the parameter vector is updated in a steepest descent fashion according to the stochastically evaluated gradient to find the minimum. The family of trial states should have good descriptive power and have the correct physics built in. The ground state of the two-dimensional Heisenberg model with nearest-neighbour interactions actually requires an algebraic, not exponential, decay of the bond length probability.

The optimization scheme takes the sign of the first derivatives of the energy and updates each adjustable parameter h_{ij} according to

$$\log h_{ij} = \log h_{ij} - \frac{R}{t^\alpha}\text{sign}\left(\frac{\partial\langle H\rangle}{\partial h_{ij}}\right). \tag{2.17}$$

$R \in [0, 1)$ is a random number, t is the optimization step and $\alpha > 0$ is an exponent that ensures the step size gradually becomes smaller. The random number is not mandatory for the optimization. It converges even if $R = 1$. The reason for introducing randomness in the optimization step is that when the derivatives become small the signs of their Monte Carlo estimates can be wrong due to statistical

fluctuations and computing the Hessian matrix is unreliable. The random number could act as occasional adjustments of amplitudes in the wrong direction. Besides, the random number could also speed up the convergence [Lou and Sandvik (2007)]. A significant benefit of taking the sign of the derivative and combining with the decaying function for a new optimization step is that the fluctuations in the gradient can be very large and hence can cause large detremental jumps in the configuration space but for this combined scheme the step size of optimization is bounded and thus we can avoid such problems. The system should be converged to lowest energy as the optimization is performed.

The trial wave function is not guaranteed to be close to the true ground state. It is possible that $|E(\vec{x}) - E_0| \ll 1$ even if $|\langle\psi^{trial}|\psi_0\rangle|$ is not close to one. The optimization is carried out to minimize the total energy after the system is thermalized when the average probability of finding a state $\mathcal{L}$ is proportional to its weight $W(\mathcal{L})$. We optimize the whole set of amplitudes for each power law exponent. A feature of the optimization scheme is that the amplitudes are adjusted in the decreasing direction of E and for any given set of amplitudes it can minimize to the same energy when the convergence is reached, which is clearly shown in Fig. 2.5(a). Accordingly the amplitudes are optimized to the same converged values as illustrated in Fig. 2.5(b). Hence we can guarantee that the results shown from Fig. 2.5(a) are completely optimal. We also carried out the simulations at different power law exponents and checked convergence. Based on the tests we can conclude that the results are converged to their optimum values within the error bars shown.

We test how the stochastic optimization scheme minimizes the energy by applying it to the L.D.A. trial wavefunction for the Heisenberg hamiltonian on a 1D chain $H = J\sum_{\langle ij\rangle} \mathbf{S}_i \cdot \mathbf{S}_j$. We start from different form of bond amplitudes $h_{ij} = h(r_{ij}) = r_{ij}^{-p}$ where p is the power law exponent and optimize the whole set of variational

parameters (see Fig. 2.5(b)). With more optimization steps, the energy is moving towards the exact ground state energy $\frac{1}{4} - \log 2$ no matter what the starting point is, which is clearly shown in Fig. 2.5(a). The results confirm that an RVB state is at least not far energetically from the ground state. In addition the optimization scheme is verified as effective and can generate the converged value that has little dependence on the initialized amplitudes.

2.2 Short bond spin liquid calculation

Anderson [Fazekas and Anderson (1974)] proposed an RVB wavefunction for the spin liquid state. With the bond amplitude product wavefunction, unbiased calculation is performed to examine whether the spin liquid can be a good description of the true ground state.

The spin liquid calculation is done for both the checkerboard and collinear AB pattern bond basis. The bond distribution of short bond spin liquid is $h(\mathbf{r}) = \delta(|\mathbf{r}| - 1)$ on the checkerboard AB pattern and $h(\mathbf{r}) = \delta(|\mathbf{r}| - \sqrt{2})$ on the collinear AB pattern, which excludes long range bonds.

2.2.1 Worm algorithm

The previous update method is achieved through exchanging bond ends of two sites: for site i in bond (i, j) and site i_2 in bond (i_2, k), new bonds are formed as (i, k) and (i_2, j). This reconfiguration is accepted with a probability of $P = h_{ij} \cdot h_{i_2,k} / h_{i,k} \cdot h_{i2,j}$. Usually it involves long bonds through reconfiguration but in short bond spin liquid Monte Carlo sampling, long bonds are given zero weights which therefore makes the probability zero or impossible to evaluate. The sampling process will become stuck

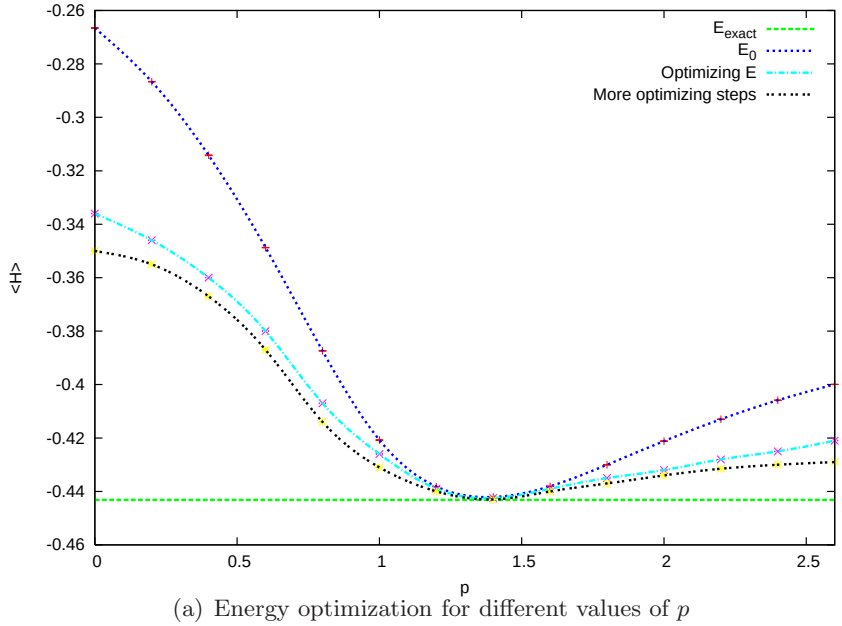

(a) Energy optimization for different values of p

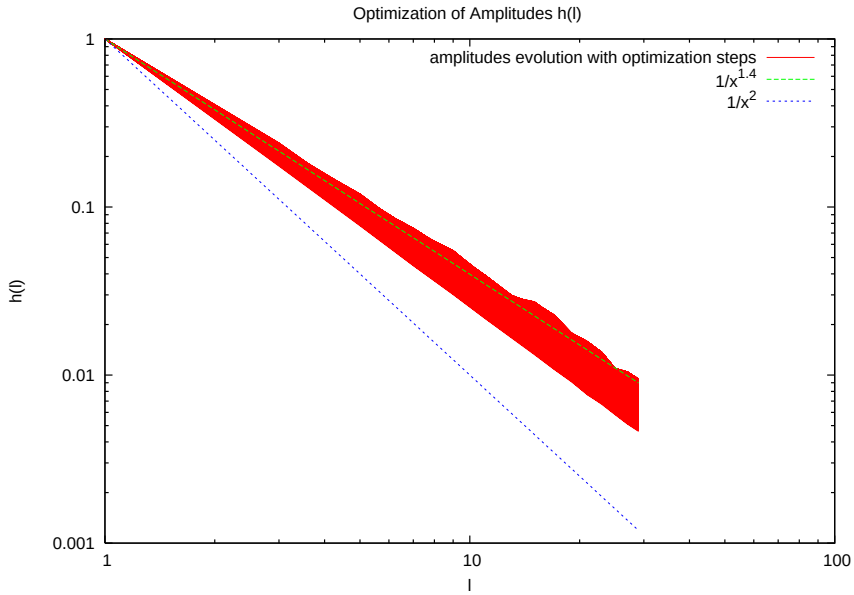

(b) Optimization of bond amplitudes starting with $p = 2.0$

Figure 2.5: The stochastic optimization scheme is tested on 1D Heisenberg model.

in one configuration or impossible to carry out. A worm algorithm is introduced to address this sampling problem and it is allowed that only short bonds (nearest neighbor bonds) will emerge throughout update process.

The worm algorithm is frequently used in path integral Monte Carlo calculations. A permutation circle (known as worm) can be open and closed. Bond reconfiguration is done at each step the worm moves. The basic update scheme is as follows:

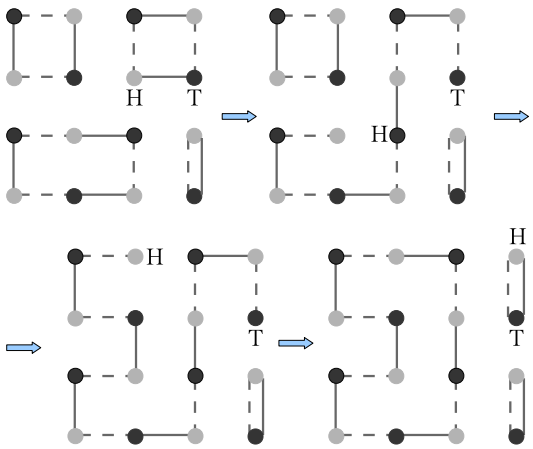

Figure 2.6: Worm update scheme: H = Head, T = Tail. The Head site moves at each step while the Tail site remains fixed. The worm stops when the Head site moves to the Tail site and a new bond configuration is formed.

1. Select a lattice site i at random (uniformly).

2. Remove the bond emerging from site i to open the permutation, i is the Head of the worm at this step and the site that previously connected to i is fixed as the Tail of the worm.

3. Select j from distribution $h_{ij}/\sum h_{ij}$ where j is one of the four nearest neighbours in short bond spin liquid calculation.

4. Draw bond from i to j with certain probability.

5. Erase the bond that was previously at j and the site that previously connected to j becomes the new Head.

6. Repeat steps $3 \rightarrow 4 \rightarrow 5$. Exit if the Head and Tail (the initial site connected with i) coincide and the worm sweep is completed.

The probability of moving from site i to site j is $P_{ij} = \frac{h_{ij}}{\sum_x h_{ix}}$. The worm algorithm's Markov chain is aperiodic and satisfies the detailed balance.

In this special case of short bond spin liquid calculation, all nearest neighbour (NN) bonds are given uniform weight. Thus the acceptance rate is reduced to be only related to loop structure; when loop splits or loop number conserves, the update is accepted with probability $P = 1$, when 2 loops join into 1, the update is accepted with probability $P = \frac{1}{2}$.

2.3 Measurement of observables

Expectation values of observables in the trial state can be interperated as an ensemble average of the estimator. The ground state at small J_2 retains classical Néel order in which the spins align in antiparallel orientation for nearest neighbours in both the vertical and horizontal directions, and the magnetic wave vector is $\mathbf{Q} = (\pi, \pi)$. The collinear state, which appears at large values of J_2, has magnetic wave vector $\mathbf{Q} = (\pi, 0)$ or $\mathbf{Q} = (0, \pi)$ and spins are antiparallel aligned for nearest neighbors in one of the directions (vertical or horizontal) while parallel aligned in the other direction [Richter and Schulenburg (2010)].

The Néel and the collinear long range order can be analyzed with corresponding order parameters. For the classical Néel order and collinear order, we have the square

of staggered magnetization M^2 that depends on $\mathbf{Q} = (\pi, \pi)$ and $(\pi, 0)$ respectively:

$$M^2 = \frac{1}{N^2} \sum_{\mathbf{r},\mathbf{r}'} e^{i\mathbf{Q}(\mathbf{r}-\mathbf{r}')} \langle \mathbf{S}_\mathbf{r} \cdot \mathbf{S}_{\mathbf{r}'} \rangle = \frac{1}{N^2} \sum_{\mathbf{r},\mathbf{r}'} (-1)^{\mathbf{r}-\mathbf{r}'} \langle \mathbf{S}_\mathbf{r} \cdot \mathbf{S}_{\mathbf{r}'} \rangle \tag{2.18}$$

For the intermediate phase we have $\hat{D}_x^2$ that depends on $\mathbf{Q} = (\pi, 0)$, i.e.

$$\hat{D}_x^2 = \frac{1}{N^2} \sum_{\mathbf{r},\mathbf{r}'} e^{i\mathbf{Q}(\mathbf{r}+\mathbf{r}')} \langle \mathbf{S}_\mathbf{r} \cdot \mathbf{S}_{\mathbf{r}'} \cdot \mathbf{S}_{\mathbf{r}+\mathbf{x}} \cdot \mathbf{S}_{\mathbf{r}'+\mathbf{x}} \rangle = \frac{1}{N^2} \sum_{\mathbf{r},\mathbf{r}'} (-1)^{r_x + r'_x} \langle \mathbf{S}_\mathbf{r} \cdot \mathbf{S}_{\mathbf{r}'} \cdot \mathbf{S}_{\mathbf{r}+\mathbf{x}} \cdot \mathbf{S}_{\mathbf{r}'+\mathbf{x}} \rangle \tag{2.19}$$

and the corresponding counterpart $\hat{D}_y^2$ to measure a bond pattern with broken translational symmetry in either direction.

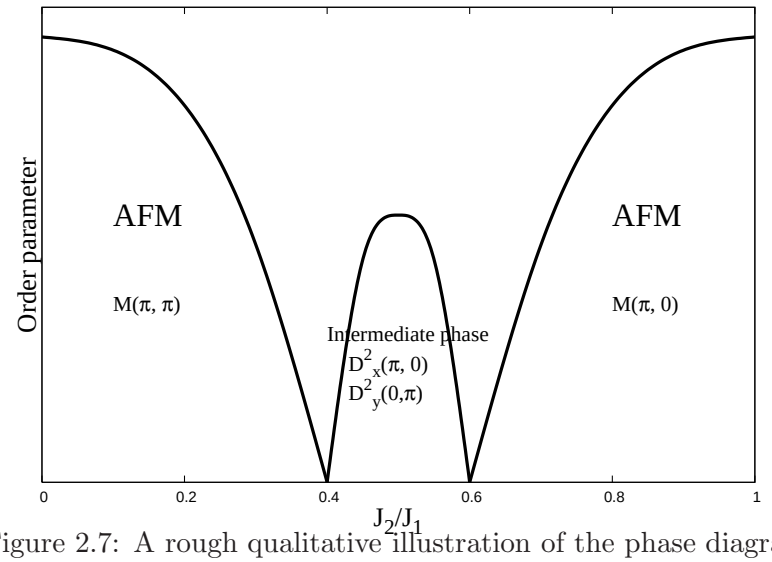

Figure 2.7: A rough qualitative illustration of the phase diagram

The transition from magnetic ordered to disordered phase can be detected through the square of Néel order parameter M^2, meanwhile the increase of D^2 will indicate the emergence of collinear order (see Fig. 2.7). From the change of order parameter we may have a clue about the order of the phase transition.

CHAPTER 3

Numerical and analytical results

We developed various numerical calculations to investigate the physics of the intermediate region (corresponding to $0.4 \lesssim J_2/J_1 \lesssim 0.6$). We approached from both sides, i.e. starting from small J_2/J_1 values and large J_2/J_1 values in bases constructed from the checkerboard and collinear AB patterns. Some evidence of the phase transition can be seen in measurements of the ground state energy and order parameters.

Different from the predictions of the ground state in the intermediate region, no supportive evidence of obvious symmetry breaking or spin liquid state was obtained from our results of various numerical calculations. Instead a 1D-like description of the ground state might be concluded from different numerical calculations.

3.1 Extending L.D.A. trial wavefunction

3.1.1 Unbiased optimization scheme results

The original L.D.A. trial wavefunction retains the full symmetry of the bond amplitudes. On a 4×4 lattice, only two kinds of bond amplitudes can be evolved, i.e. $h(|\mathbf{r}| = 1)$ and $h(|\mathbf{r}| = 3)$ where $|\mathbf{r}|$ is measured in Manhattan length. Thus the probability of each bond configuration is only determined by the ratio of these two bond amplitudes then we can tune the ratio to approach the lowest energy state. According to the power law form of the bond amplitude in L.D.A. trial wavefunction, the bond amplitude decreases as the bond becomes long-ranged so it is reasonable to keep the ratio less than 1. Furthermore the ratio should also remain positive to make the update of bond configuration possible. The ratio is tuned continuously from 0.01 to 0.9 (see Fig. 3.1). No local minimum has been achieved beyond $J_2/J_1 = 0.4$, which means this original form of trial wavefunction is no longer suitable for variational calculation and we need to propose an extended form of the trial wavefunction to solve the problem.

We first add in more degrees of freedom for the L.D.A. trial wavefunction by allowing the bond amplitude changing as $h(\mathbf{r}) = h(|x|, |y|)$ with reflection symmetry retained. Thus the total number of variational parameters grows quadratically instead of linearly with lattice size: changing from $\frac{L}{2}$ to $\frac{L^2}{8} + \frac{L}{2}$ (checkerboard AB pattern) or $\frac{L^2}{8} + \frac{L}{4}$ (collinear AB pattern) for an $L \times L$ lattice. The set of variational parameters evolve through stochastic optimization until convergence is achieved.

Each $h(\mathbf{r}_{ij})$ is updated by minimizing the energy estimator. The stochastic optimization scheme has an optimization step size which is tuned smaller with the time step. The convergence criteria is set to be a sufficiently small value between the

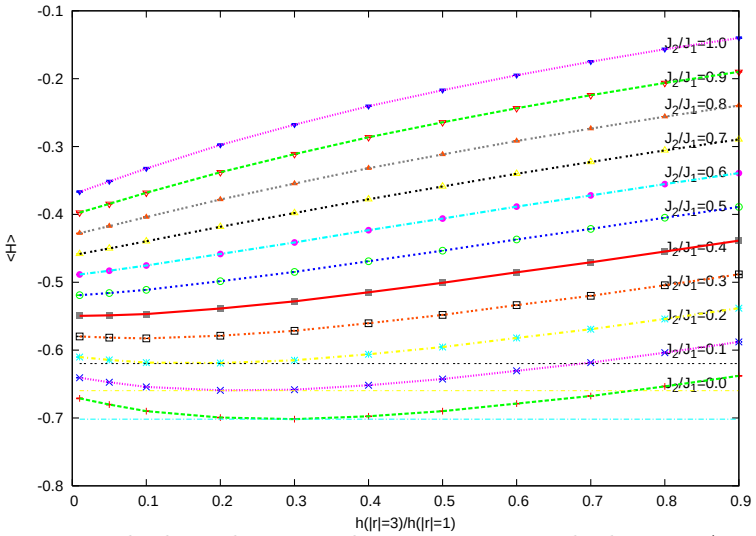

Figure 3.1: We calculate the ground state energy with the L.D.A. type trial wavefunction for checkerboard AB pattern on 4×4 lattice.

difference of two successive optimized values of variational parameters, which may be artificial as the step size is manually tuned to be decreasing with time. To solve this problem, the optimization is done iteratively to ensure genuine convergence. The bond amplitudes are given an initial value of $h(\mathbf{r}_{ij}) = r^{-p}$ where r is the Manhattan distance between site i and j. A new set of optimized value obtained from the first run serves as the input for the next optimization process. The energy is lowered through this iterative process and convergence can be reached when the output values of two successive optimization runs agree within error.

The unbiased optimization calculations are performed for both checkerboard and collinear AB patterns on 4×4, 8×8, 16×16 and 32×32 square lattices. Evidence of a transition can be found through the measurements of observables; the ground state energy increases with frustration on checkerboard AB pattern and decreases on the collinear AB pattern, staggered magnetization $M^2(\pi,\pi)$ and $M^2(\pi,0)$ indicate the AFM phase for both small J_2/J_1 and large J_2/J_1 region and the dimer correlation

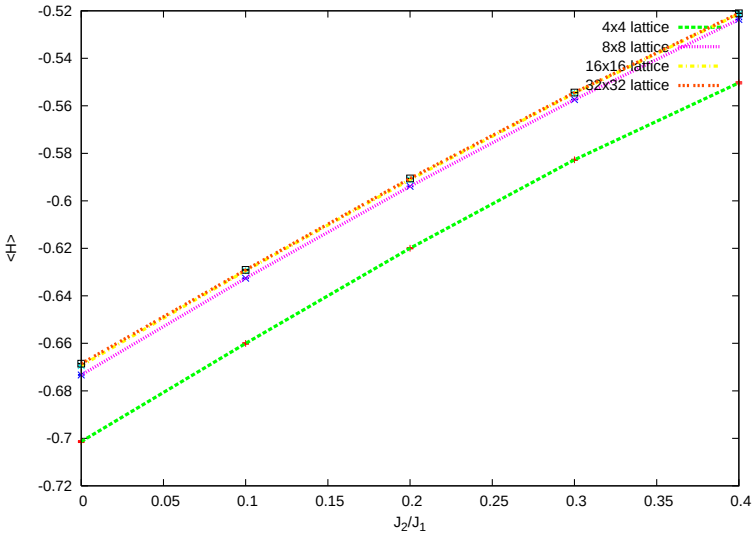

Figure 3.2: Energy results from the unbiased optimization calculation with the checkerboard AB pattern bond basis on different lattice sizes (4×4, 8×8, 16×16, 32×32)

D^2 increases in the intermediate phase region but shows some large fluctuation, which is not exactly what we expected. The 4×4 lattice calculation results show an agreement with exact diagonalization results on ground state energy for small J_2/J_1 (see Fig. 3.11). The slight discrepancy from the collinear AB pattern results may be due to the fact that the $h(1,3)$ bond can not be involved because of the periodic boundary condition. Exact calculation data of larger lattice size is not available for us to compare.

The calculation results for different lattice sizes with checkerboard and collinear AB pattern are presented as Figs. 3.2, 3.3, 3.4, 3.5. The ground state energy results of the intermediate phase region are approached from both sides, i.e. small J_2/J_1 value with checkerboard AB pattern and large J_2/J_1 value with collinear AB pattern. Across the entire range the energy initially increases with frustration then decreases. With the lattice size growing, the energy results rapidly converge. The

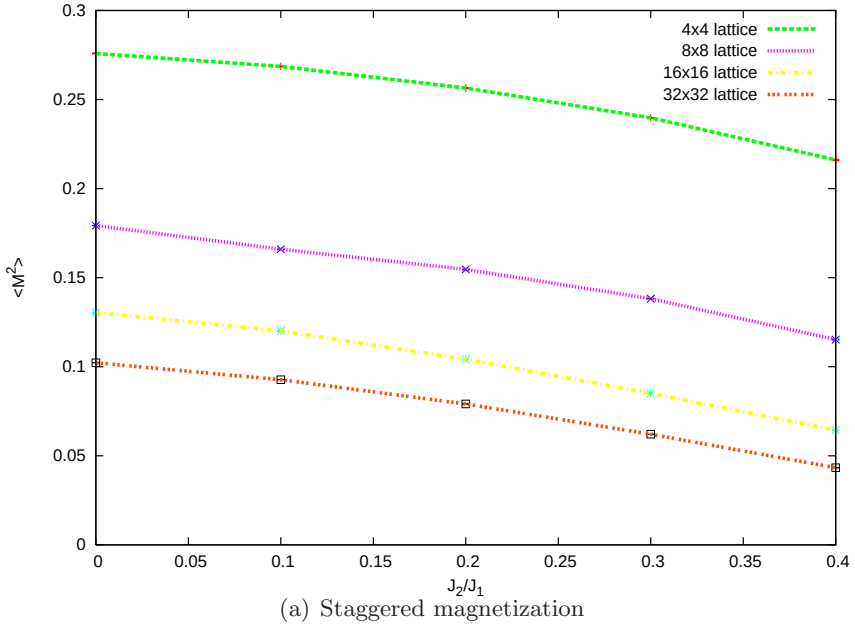

(a) Staggered magnetization

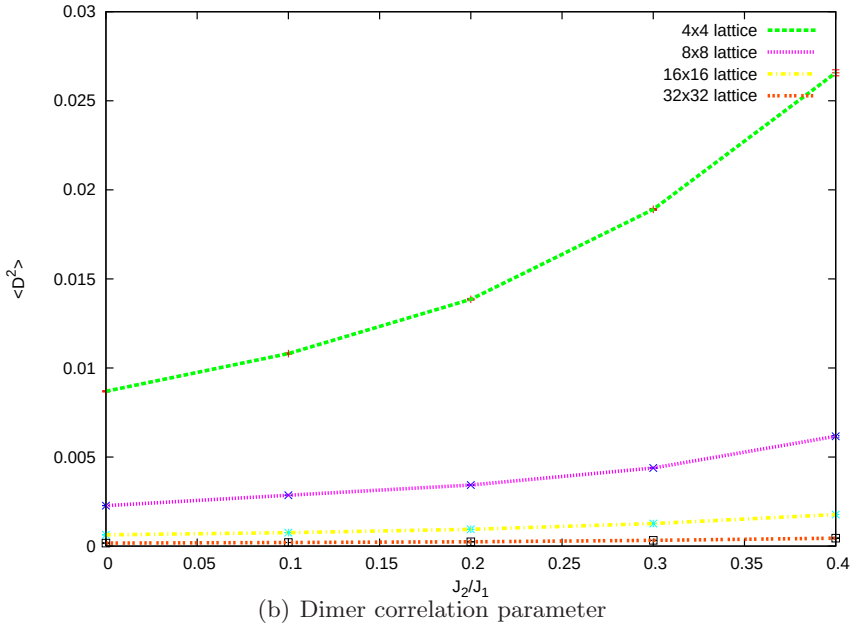

(b) Dimer correlation parameter

Figure 3.3: Order parameter results from different lattice sizes (4×4, 8×8, 16×16, 32×32) with checkerboard AB pattern

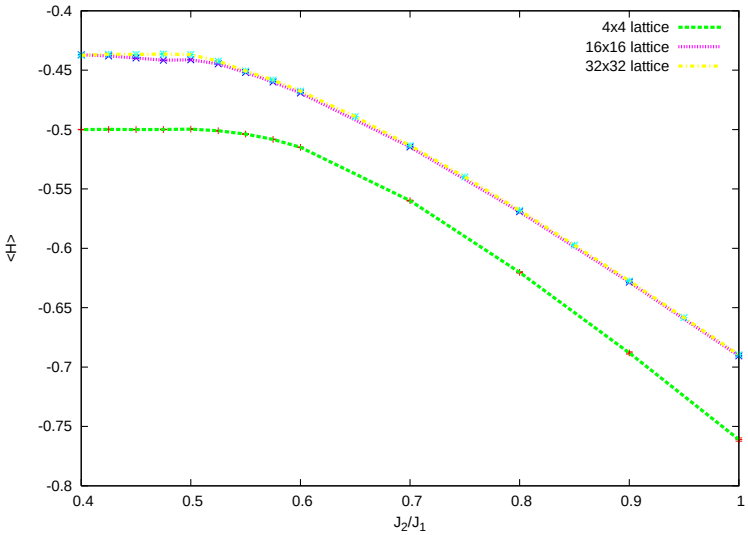

Figure 3.4: Energy results from the unbiased optimization calculation with the collinear AB pattern bond basis on different lattice sizes

staggered magnetization is found to be gradually killed as the intermediate region is approached, which agrees with our predictions. The dimer correlation parameter increases in the intermediate region; however with the lattice size growing it shows a steady convergence towards zero in the thermodynamic limit. The dimer correlation parameter can effectively detect ordered bond alignments. Thus this result may imply that the proposed bond patterns in the valence bond crystal state do not emerge in the intermediate phase region.

The optimization scheme shows how the bond amplitudes evolve through approaching the minimum energy state in the variational calculation. In the checkerboard case, the bond amplitudes gradually exhibit a different tendency as J_2/J_1 approaches to the intermediate phase region; they decay much less rapidly along the main axis than other directions (see Fig. 3.6(c),3.6(d)), and at the end of the optimization the bond amplitudes along x-axis and y-axis still have relatively large amplitudes. This again confirms that the simple power-law form of bond amplitudes in L.D.A. trial

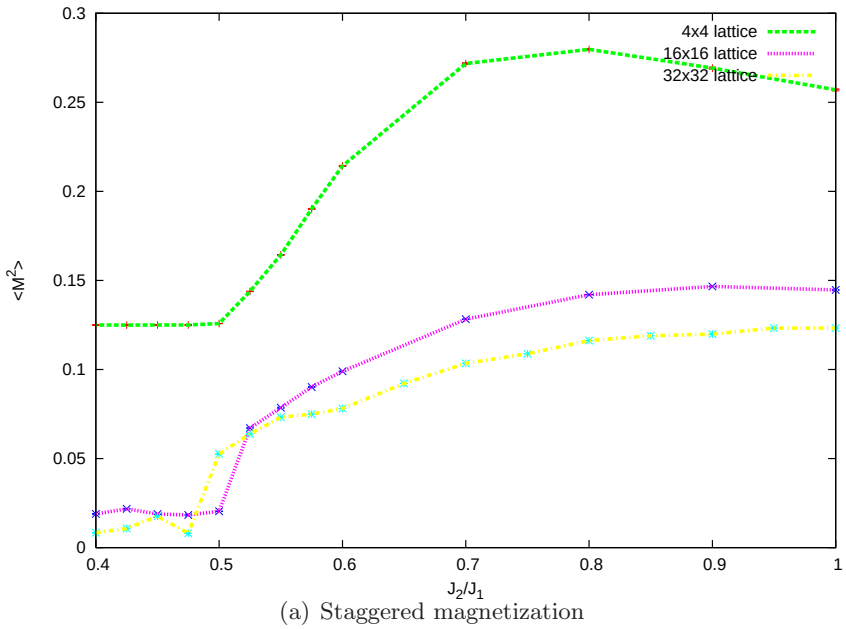

(a) Staggered magnetization

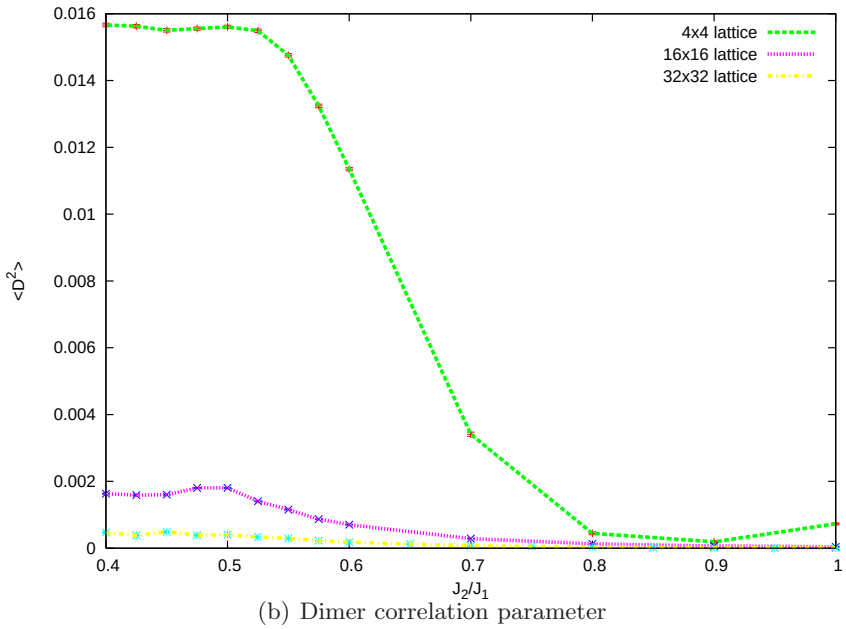

(b) Dimer correlation parameter

Figure 3.5: Order parameters results from the unbiased optimization calculation with the collinear pattern bond basis on different lattice sizes (4×4, 16×16, 32×32)

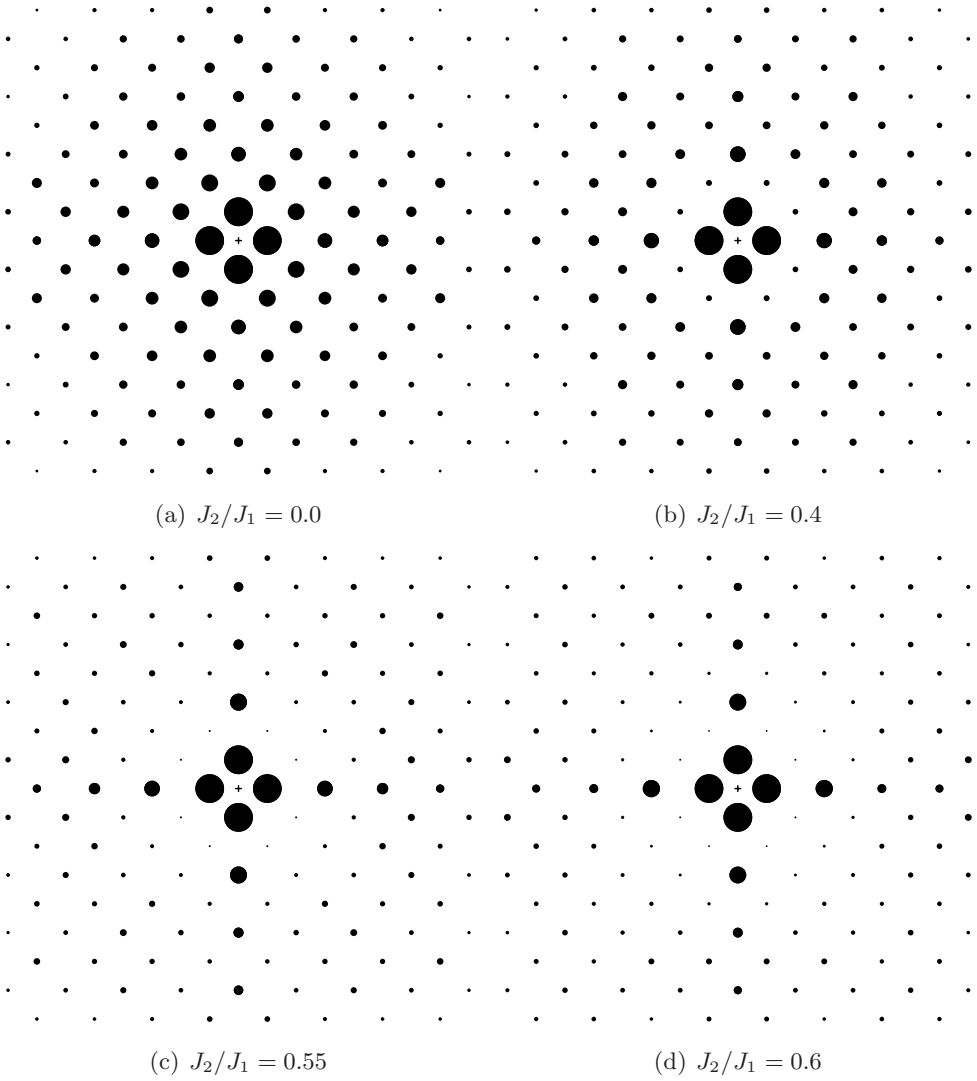

(a) $J_2/J_1 = 0.0$ (b) $J_2/J_1 = 0.4$

(c) $J_2/J_1 = 0.55$ (d) $J_2/J_1 = 0.6$

Figure 3.6: Bond amplitudes calculated from unbiased optimization scheme for checkerboard lattice pattern. Starting from the center of figure, the center of circles denote the ending points of bonds. The area of circles is proportional to $|h(\vec{\mathbf{r}})|$.

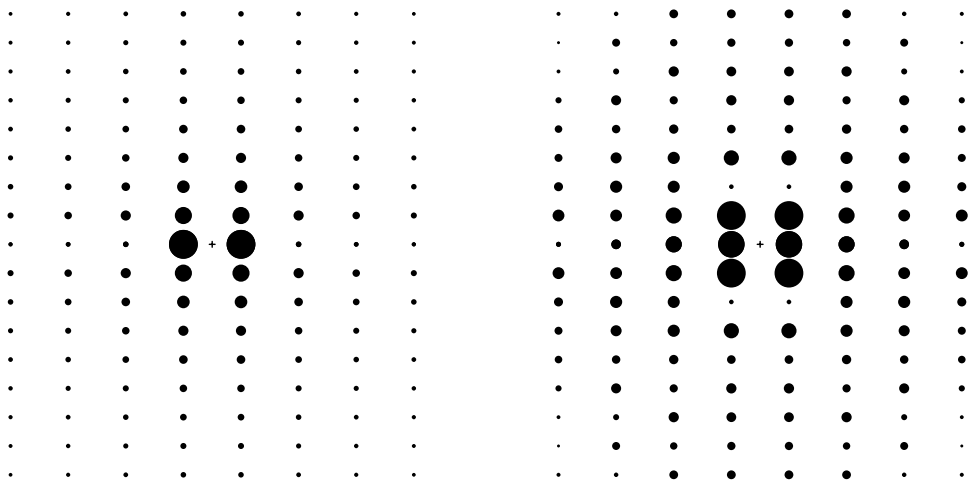

(a) Initial bond pattern (b) Final bond pattern

Figure 3.7: Results of bond amplitudes from unbiased calculation at $J_2/J_1 = 1.0$ for collinear AB pattern on 16×16 lattice. Bond pattern initialized as $h(\mathbf{r}_{ij}) = |\mathbf{r}_{ij}|^{-3}$ evolves with optimization. Bonds are drawn as starting from centre cross ending in each circle centre. The area of circles is proportional to bond amplitudes.

wavefunction is no longer able to effectively represent the actual bond distribution when frustrating interactions are introduced. Another important behaviour shown in these figures is that the bond amplitudes $h(1,2)$ and $h(2,1)$ in checkerboard AB pattern bond basis (see Fig. 3.6) and $h(1,2)$ in collinear AB pattern bond basis (see Fig. 3.7) move towards zero in the intermediate phase region, which implies this bond amplitude may actually be tending negative.

3.1.2 Master equation for computing bond amplitudes

Mean-field-like techniques are available that make predictions about the $h(\mathbf{r}_{ij})$ parameters. We start from the amplitude product trial wave function

$$|\Psi\rangle = \sum_{\alpha} \prod_{i\in A, j\in B} h(\mathbf{r}_{ij})|V_{\alpha}\rangle \tag{3.1}$$

and assume that the state $|\Psi\rangle$ will gradually form a steady distribution under a restricted quantum evolution [Beach (2009)] in the $\tau \to \infty$ imaginary time limit. We thus write

$$|\Psi(\tau)\rangle = e^{-\tau\hat{\mathcal{F}}\hat{\mathcal{H}}\hat{\mathcal{F}}}|\Psi(0)\rangle. \tag{3.2}$$

We have a propagator $e^{-\tau\hat{\mathcal{F}}\hat{\mathcal{H}}\hat{\mathcal{F}}}$ where $\hat{\mathcal{H}}$ is frustrated Heisenberg hamiltonian and $\hat{\mathcal{F}}$ is a projection onto the space of RVB wavefunctions.

In contrast to the variational method, in which the bond amplitudes are optimized by minimizing the ground state energy, we can derive a master equation that determines how the bond amplitudes evolve at each short time step $\Delta\tau$.

With the bond operator $P_{ij} = \frac{1}{4} - \mathbf{S}_i \cdot \mathbf{S}_j$ acting on two nearest neighbour sites i and j, valence bonds can either be reconfigured or unchanged:

$$P_{ij}(i,k)(i_2,j) = \frac{1}{2}(i,j)(i_2,k) \tag{3.3}$$

or

$$P_{ij}(i,j)(i_2,k) = (i,j)(i_2,k) \tag{3.4}$$

When P_{ij} acts on two next nearest neighbour sites i and j, it will introduce non-bipartite bonds. However, the non-bipartite bonds can be excluded through the over-completeness relation so that we have

$$\tilde{P}_{ij}(i,k)(i_2,j) = \frac{1}{2}(i,j)(i_2,k), \tag{3.5}$$

with $\tilde{P}_{ij} = \frac{1}{4} + \mathbf{S}_i \cdot \mathbf{S}_j = \frac{1}{2} - P_{ij}$. Similar to the master equation for checkerboard lattice pattern [Beach (2009)], which includes the effects of the bond operator, an analytical master equation can be obtained for the collinear AB pattern corresponding to the bond reconfiguration process.

$$\dot{h}(\mathbf{r}) = \sum_{\mathbf{a}=\pm\vec{x}} [\delta_{\mathbf{a},\mathbf{r}} + \sum_{\mathbf{r}',\mathbf{r}''} \delta_{\mathbf{r}'+\mathbf{r}''-\mathbf{a},\mathbf{r}} h(\mathbf{r}')h(\mathbf{r}'')] - zh(\mathbf{r}) \tag{3.6}$$

$$+ \sum_{\mathbf{a}=\pm\vec{y}} \sum_{\mathbf{r}',\mathbf{r}''} [\delta_{\mathbf{r}'+\mathbf{a},\mathbf{r}} + \delta_{\mathbf{r}''-\mathbf{a},\mathbf{r}}] h(\mathbf{r}')h(\mathbf{r}'') - zh(\mathbf{r}) \tag{3.7}$$

$$+ \frac{J_2}{J_1} \{ \sum_{\tilde{\mathbf{a}}} [\delta_{\tilde{\mathbf{a}},\mathbf{r}} + \sum_{\mathbf{r}',\mathbf{r}''} \delta_{\mathbf{r}'+\mathbf{r}''-\tilde{\mathbf{a}}} h(\mathbf{r}')h(\mathbf{r}'')] - 2\tilde{z}h(\mathbf{r}) \} \tag{3.8}$$

where $d = 2$ is the dimension of the lattice, $z, \tilde{z}$ are the coordinate number $z = 2d$

and $\tilde{z} = 2^d$. The Fourier transformation of the master equation gives

$$\frac{1}{z}\dot{h}_{\mathbf{q}} = \gamma_{q_x} + \gamma_{q_x} h_{\mathbf{q}}^2 + 2\gamma_{q_y} h_{\mathbf{q}} - 2h_{\mathbf{q}} \tag{3.9}$$

$$+ g(\tilde{\gamma}_{\mathbf{q}} + \tilde{\gamma}_{\mathbf{q}} h_{\mathbf{q}}^2 - 2h_{\mathbf{q}}). \tag{3.10}$$

where $\tilde{z} = 2^d$, $\gamma_{q_y} = \frac{1}{d}\cos k_y$, $\tilde{\gamma}_{\mathbf{q}} = \cos k_x \cos k_y$ and $g = \frac{J_2}{J_1}\frac{\tilde{z}}{z}$. We can solve this equation for the steady distribution and have

$$h_{\mathbf{q}} = \frac{\Lambda_{\mathbf{q}} - [\Lambda_{\mathbf{q}}^2 - (\gamma_{q_x} + g\tilde{\gamma_{\mathbf{q}}})^2]^{\frac{1}{2}}}{\gamma_{q_x} + g\tilde{\gamma_{\mathbf{q}}}} \tag{3.11}$$

where $\Lambda_{\mathbf{q}} = g + 1 + \gamma_{q_y}$.

Unlike in the unbiased optimization scheme applied in the VMC calculation, the bond amplitude $h(\mathbf{r})$ is free to move toward either positive or negative values in the master equation calculation results. With the Marshall's sign rule potential broken due to frustration, the ground state no longer has a positive definite expansion; thus the bond amplitudes can be negative. This can not be achieved in the VMC calculation since the bond amplitude is actually updated as $h(\mathbf{r})_{n+1} := h(\mathbf{r})_n \cdot e^{\text{factor}}$, and hence $h(\mathbf{r})$ always remains positive. In addition, bond amplitudes are involved in calculating the acceptance rate in bond reconfiguration of each Monte Carlo sampling step, so only positive bond amplitudes ensure that the sampling process can carry on. As a result, bond amplitude that turns to negative with the increase of frustration are thus moving towards zero in Monte Carlo calculation.

One of the advantages of calculating bond amplitudes from master equation rather than unbiased optimization in VMC method is that it requires much less time and computation power since it runs without the time-consuming optimization step. It is easy to calculate the bond amplitude distribution for various lattice sizes, so it is

convenient to obtain a clear idea of the bond amplitude distribution for sufficient large lattice like 128×128.

For the checkerboard AB pattern at small values of J_2/J_1, the unbiased optimization scheme gives the bond amplitudes shown in Fig. 3.6. As frustration increases, the $h(1,2)$ (or equivalently $h(2,1)$) bond amplitude decays rapidly towards zero, which is consistent with the master equation calculation results [Beach (2009)]. From the master equation results, the bond amplitudes exhibit a 1D-like behavior. The bond amplitudes do not show a tendency to become strictly short ranged as the frustration increases. In contrast, the bonds become long ranged along x-axis and y-axis, while bond amplitudes in other directions fall off rapidly (faster than power-law) as the J_2/J_1 value approaches the intermediate region. This has been verified by our unbiased calculation (see Figs. 3.6 and 3.7).

The strict positivity of the bond amplitudes demonstrates the region where the Marshall's sign rule holds. The collinear AB pattern corresponds to the Marshall's sign rule for large J_2. All bond amplitudes become positive above $J_2/J_1 = 5.23$. Bond $h(1,2)$ turns negative first as J_2/J_1 decreases. Additional bonds turn negative for smaller J_2/J_1 values, which indicates the Marshall sign rule is thoroughly broken.

With the bond amplitudes derived from the master equation as the initial value, we can perform Monte Carlo sampling. Since negative bond amplitudes will emerge when $J_2/J_1 \leq 5.23$ for collinear AB pattern on 16×16 lattice, this may lead to negative probability through sampling. However, we can still perform unbiased calculations while the sign problem is not too severe, i.e. only a handful of the h amplitude is negative. We separate the sign and the amplitude, the sign part ϵ is absorbed into the observable $\hat{O}$ and we sample with probability distribution $|\omega|$. Thus what we actually have is

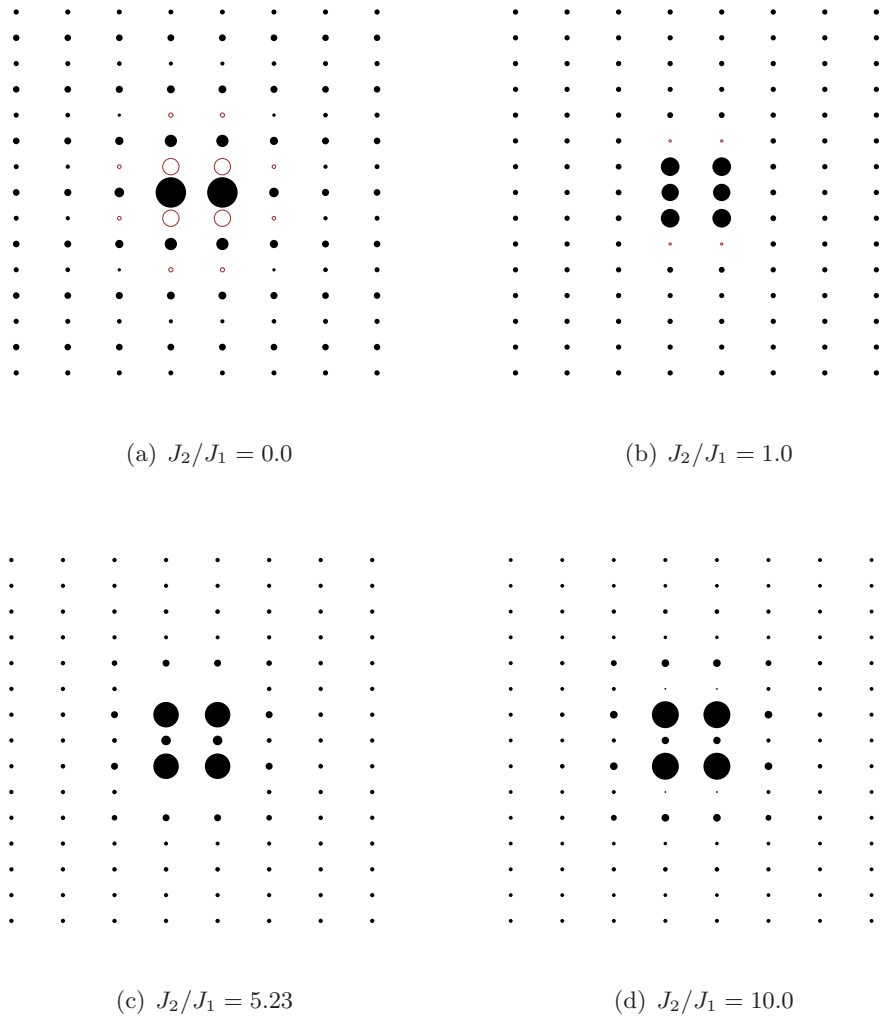

(a) $J_2/J_1 = 0.0$ (b) $J_2/J_1 = 1.0$

(c) $J_2/J_1 = 5.23$ (d) $J_2/J_1 = 10.0$

Figure 3.8: Bond amplitudes are shown as black circles for positive value, red empty circles for negative value. Starting from the center of figure, the center of circles denote the ending points of bonds. The area of circles is proportional to $|h(\vec{\mathbf{r}})|$.

$$\langle \hat{O} \rangle = \frac{\sum_{\alpha' \alpha} \langle V_{\alpha'} | V_\alpha \rangle \frac{\langle V_{\alpha'} | \hat{O} | V_\alpha \rangle}{\langle V_{\alpha'} | V_\alpha \rangle}}{\sum_{\alpha' \alpha} \langle V_{\alpha'} | V_\alpha \rangle} = \frac{\sum \epsilon |\omega| O}{\sum \epsilon |\omega|} \tag{3.12}$$

$$= \frac{\sum |\omega| (\epsilon O)}{\sum |\omega|} \cdot \frac{\sum |\omega|}{\sum |\omega| \epsilon} = \frac{\langle \epsilon \hat{O} \rangle_{|\omega|}}{\langle \epsilon \rangle_{|\omega|}} = \frac{\sum_i \epsilon_i O_i}{\sum_i \epsilon_i}. \tag{3.13}$$

We can still obtain meaningful results through this sampling scheme with slight sign problem.

3.1.3 Monte Carlo sampling with master equation results

The master equation for the collinear AB pattern bond basis provides an approximation of bond amplitudes for the factorizable wavefunction. Thus we can obtain information about the ground state properties through sampling with these sets of bond amplitudes. Since the Marshall sign rule can only be fulfilled for large J_2/J_1 values, a sign problem exists for $J_2/J_1 < 5.23$. The sign expectation $\langle \epsilon \rangle$ in Eqn. 3.12 can be evaluated in the sampling process (see Fig. 3.9). For ground states which have positive definite expansion $\langle \epsilon \rangle$ is exactly 1. With frustration introduced in, the sign expectation will fluctuate in the range $(-1, 1)$. For large deviation from 1 the ground state energy results are no longer reliable. We present the norm of the sign expectation in Fig. 3.9, and we can see the sign problem tends to be severe in the range $(1, 2)$: the sign expectation is near zero which can lead to large fluctuation in the measurement of observables.

3.1.4 Short bond spin liquid calculation

The short bond, i.e. nearest neighbour bond, denotes the valence bond formed between two sites on the edge of a smallest plaquette for checkerboard AB pattern.

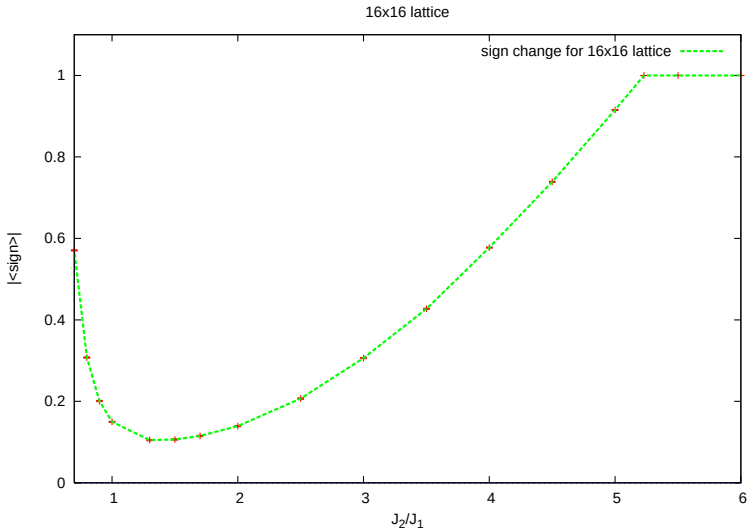

Figure 3.9: The sign expectation for the collinear AB pattern on 16x16 lattice

Whereas for collinear AB pattern which can be seen as two checkerboard ordered grids rotated 45° penetrating through each other, the short bonds thus should be those formed between the diagonal sites of a plaquette. On a $L \times L$ square lattice the $2L^2$ short bonds are given uniform weights meanwhile other bonds are give zero weights therefore will not be involved in any bond reconfiguration.

The spin liquid calculation was performed for both AB patterns on different lattice sizes (4×4, 8×8, 16×16, 32×32). The worm update is ergodic and able to keep a sufficiently large acceptance rate (0.714403 on 16×16 lattice) during the sampling. The measurement of observables shows a convergent result (see Fig. 3.10).

All nearest neighbour short bonds in the configuration exclude the presence of magnetic order which emerges in long range bond configuration. The spin liquid calculation results provides an upper bound for ground state energy.

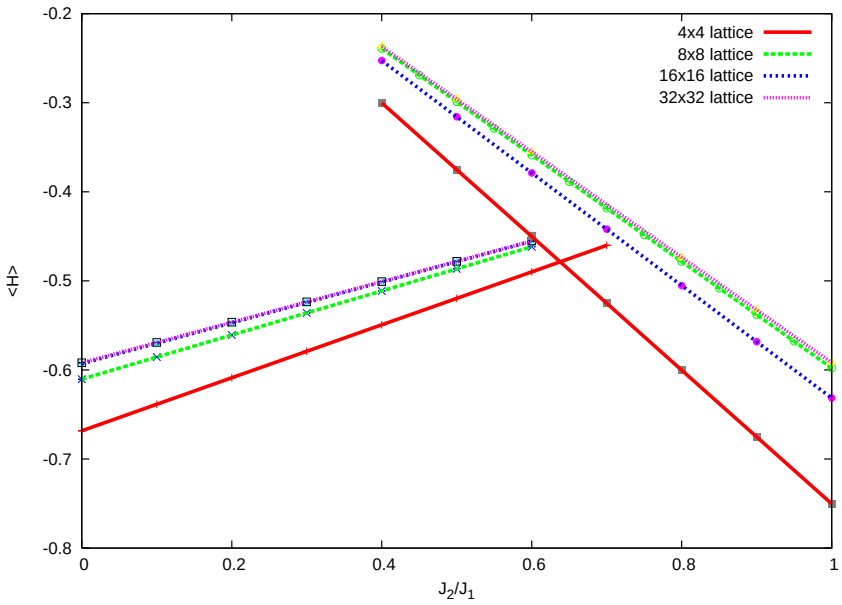

Figure 3.10: Energy expectation of spin liquid calculation for both AB patterns bond basis on different lattice size.

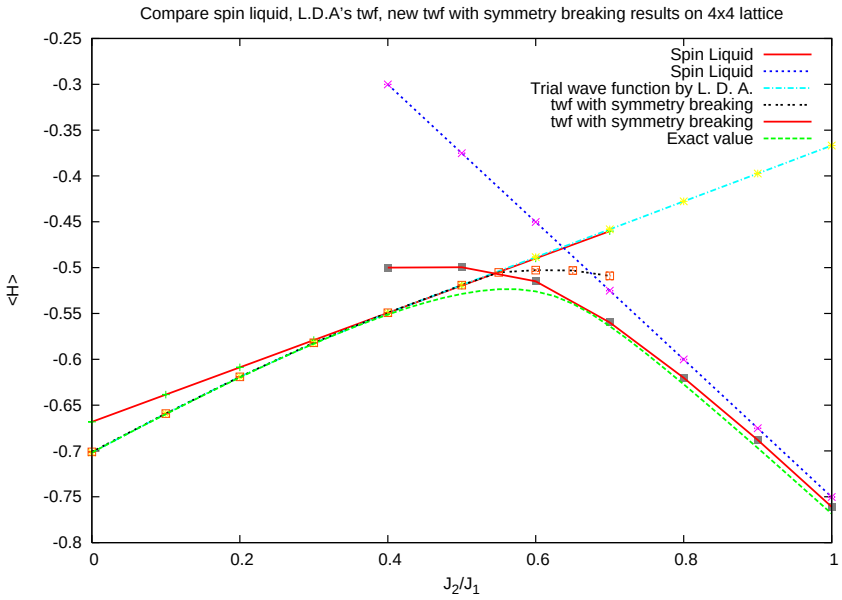

Figure 3.11: Comparison spin liquid calculation results with symmetry breaking calculation and exact value for 4×4 lattice.

3.2 Symmetry breaking calculation results

It is proposed that a columnar pattern with translational and rotational symmetry breaking or plaquette pattern with translational symmetry breaking might be the possible ground state of the intermediate region. Bonds are localized between nearest neighbours to form a crystal order, without long range magnetic order detected. This can be examined through variational Monte Carlo calculation.

We can add in explicit symmetry breaking in the trial wave function by introducing more degrees of freedom to the bond product state that take each nearest neighbour (NN) bond amplitude h_{ij} as free parameter. For long bonds we still maintain the algebraic decaying form $h_{ij} = |\mathbf{r_i} - \mathbf{r_j}|^{-p}$ to simplify the calculation. But all the NN bond amplitudes h_{ij} become adjustable parameters in the variational calculation. The size of the set of variational parameters still grows quadratically with lattice size so the calculation is not too expensive to carry out and can reach sufficiently large lattices to obtain meaningful results.

The NN bond configuration therefore can either change to a uniform pattern which returns to the original form of the trial wave function or it can change to a columnar or plaquette configuration with strong or weak bonds.

We start with different configurations to ensure that we are able to find the local minimum even in the case of a complicated energy landscape. During plaquette initialization, we define bonds on the plaquette edges as strong bonds and others as weak bonds which thus have smaller amplitudes, and in columnar initialization we define strong and weak bonds alternatively to form a columnar pattern. We also tested the uniform initialization that all bonds are given the same initial weight. Consistent results are obtained from all the different starting points (see Fig. 3.12)

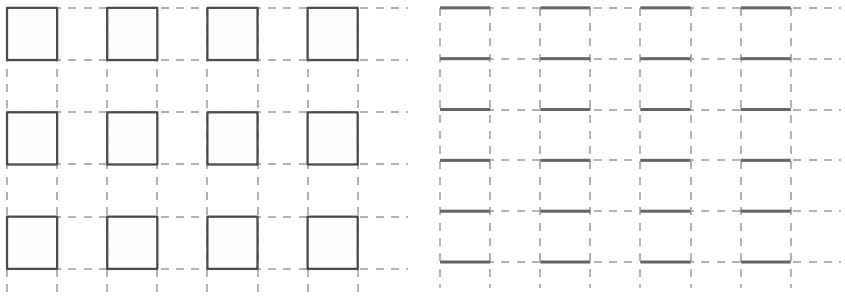

(a) Plaquette initialization (b) Columnar initialization

Figure 3.12: Two of the starting points we tried in symmetry breaking calculations. In the plaquette initialization we define bonds on each plaquette edge as strong bond (shown as dark grey line) and others as weak bond (shown as dashed light grey line). In the columnar initialization strong and weak bonds together form this columnar pattern. In the uniform initialization all NN bonds are given the same weight and thus no obvious bond pattern is formed.

which implies our optimization scheme is not stuck in any spurious local minimum of the energy landscape.

With this trial wave function, which allows spontaneous symmetry breaking, we have the uniform NN bond configuration for small values $J_2/J_1 \lesssim 0.4$ and a collinear ordered where NN bonds forms stripes for $J_2/J_1 \gtrsim 0.6$ on a 4×4 lattice. However, the rotationally symmetry breaking bond pattern is not stable; it will not emerge on larger lattice sizes 16×16. This implies that the symmetry breaking state in small lattice size is not real because small lattices tend to form some ordered RVB states.

This scheme will allow translational and rotational symmetry breaking. We did not find any obvious bond pattern with translational or rotational symmetry breaking in variational calculation results on 8×8, 16×16 and 32×32 lattices. The short bond distribution tends to be uniform without breaking any symmetry.

We find that magnetization $\langle \hat{\mathbf{M}}^2 \rangle$ is gradually killed in the intermediate region. The measurements of dimer correlation parameter $\langle \hat{\mathbf{D}}^2 \rangle$ on different lattice sizes suggest that the dimer correlation parameter converges towards zero in the thermodynamic limit.

In comparison to the symmetry breaking calculation, the unbiased optimization scheme reduces the degrees of freedom of nearest neighbours. However it still gives consistent results with the symmetry breaking calculation (see Figs. 3.13, 3.15), which implies there may not be spontaneous symmetry breaking for the ground state in phase transition region. With lattice size increasing, the results of ground state energy and order parameters approach to convergence (see Figs. 3.17, 3.19).

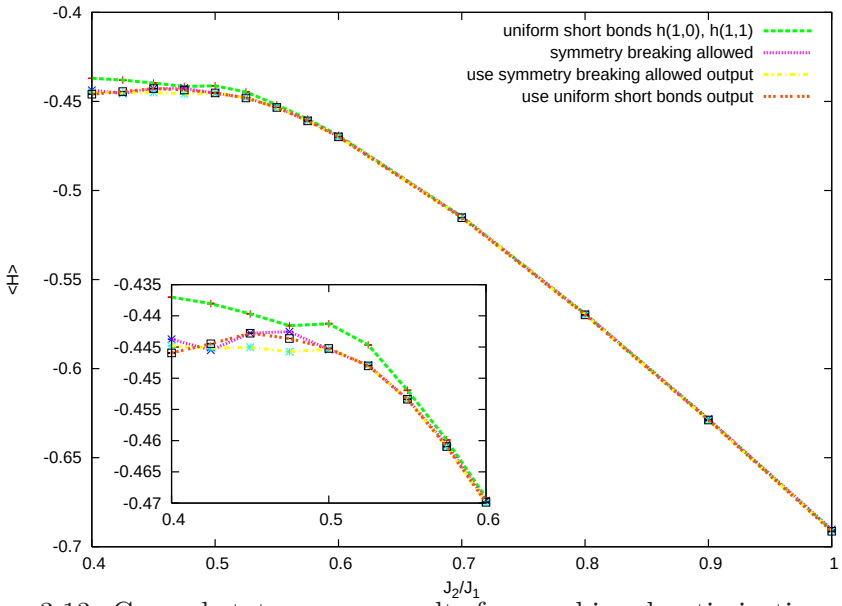

Figure 3.13: Ground state energy results from unbiased optimization calculations and symmetry breaking results on 16×16 lattice with collinear AB pattern.

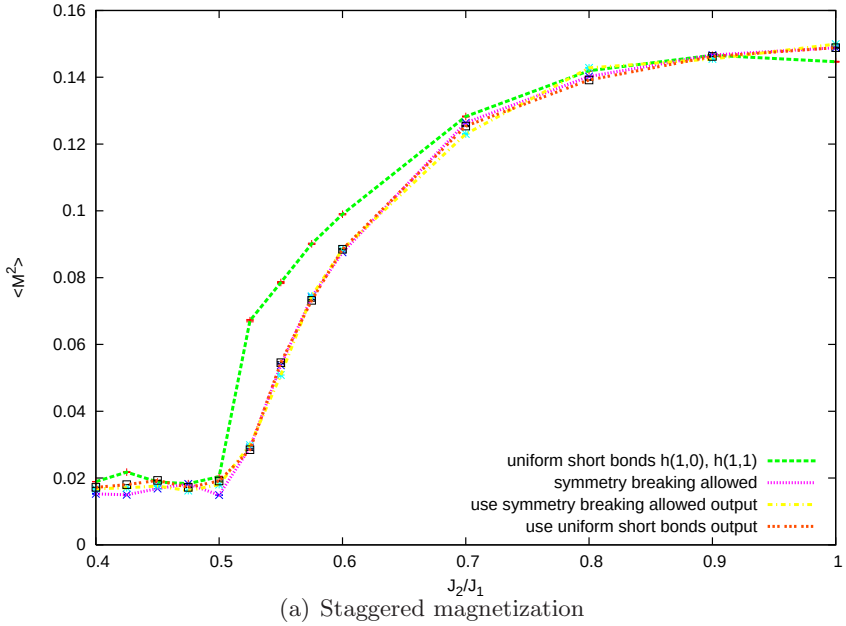

(a) Staggered magnetization

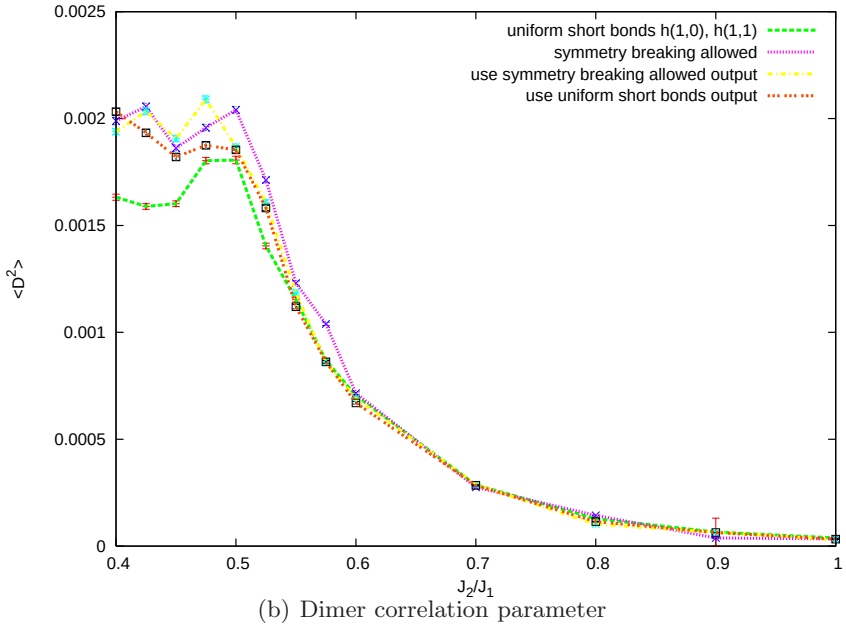

(b) Dimer correlation parameter

Figure 3.14: Converged unbiased optimization scheme gives consistent results as symmetry breaking calculation for 16×16 collinear AB pattern.

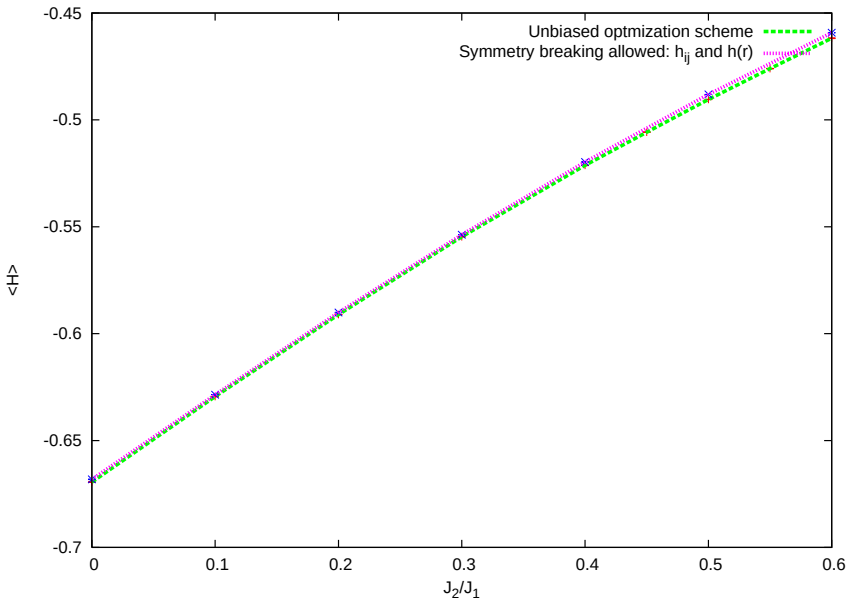

Figure 3.15: Ground state energy results from unbiased optimization calculations and symmetry breaking results on 16×16 lattice with checkerboard AB pattern.

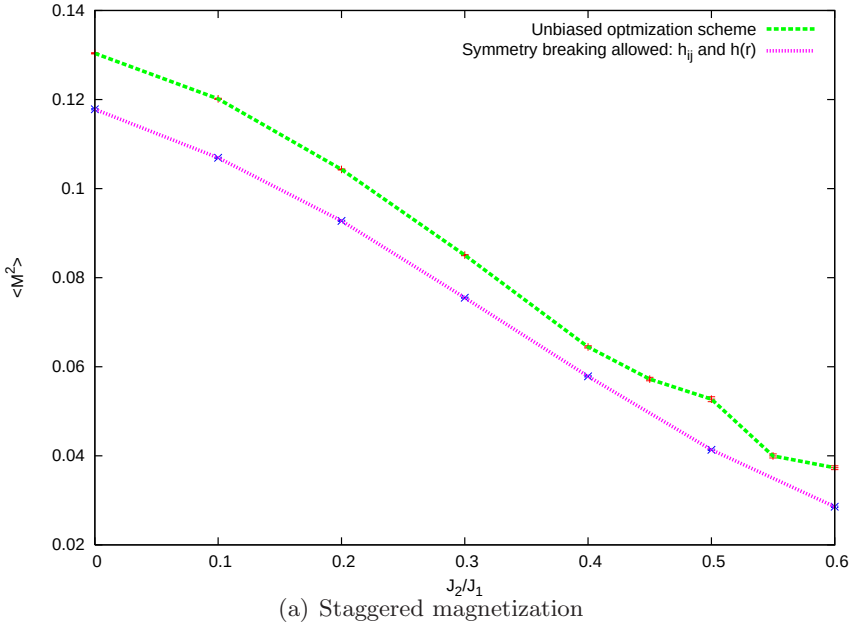

(a) Staggered magnetization

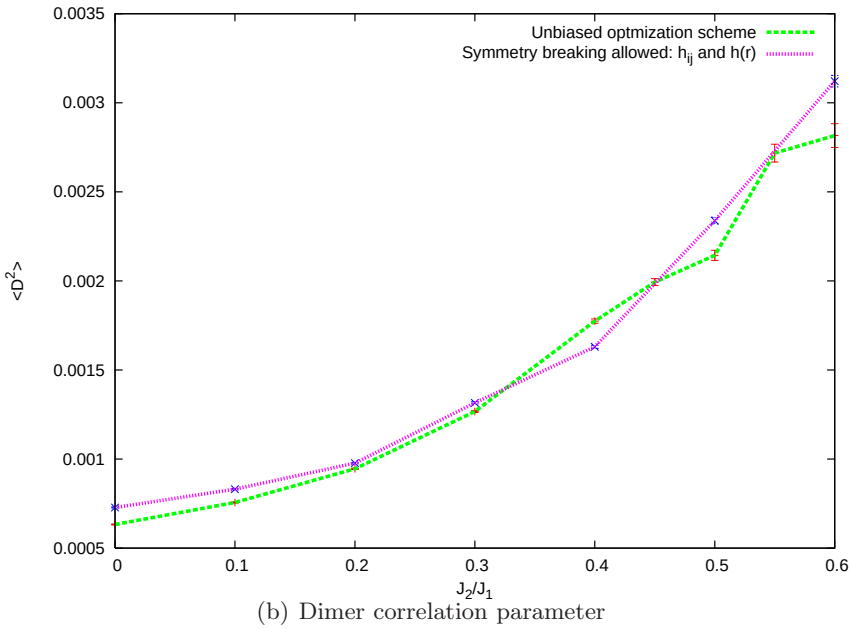

(b) Dimer correlation parameter

Figure 3.16: Converged unbiased optimization scheme and symmetry breaking calculation results for 16×16 checkerboard AB pattern bond basis.

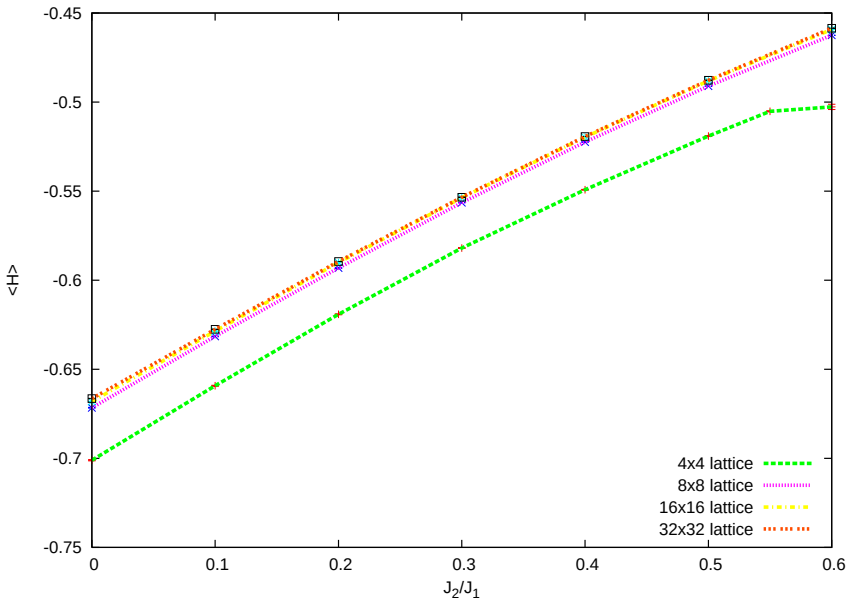

Figure 3.17: Ground state energy results from symmetry breaking calculation on 4×4, 8×8, 16×16 and 32×32 checkerboard AB pattern bond basis.

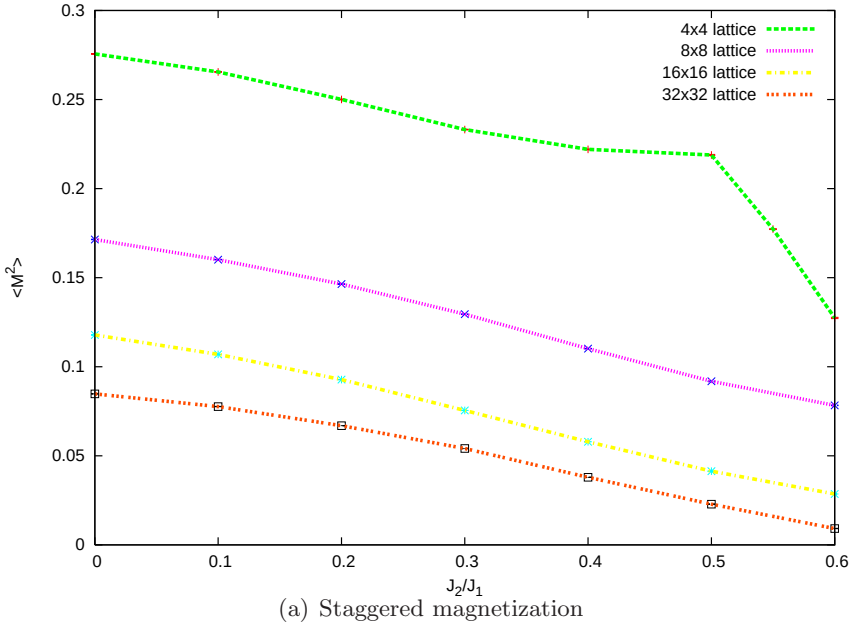

(a) Staggered magnetization

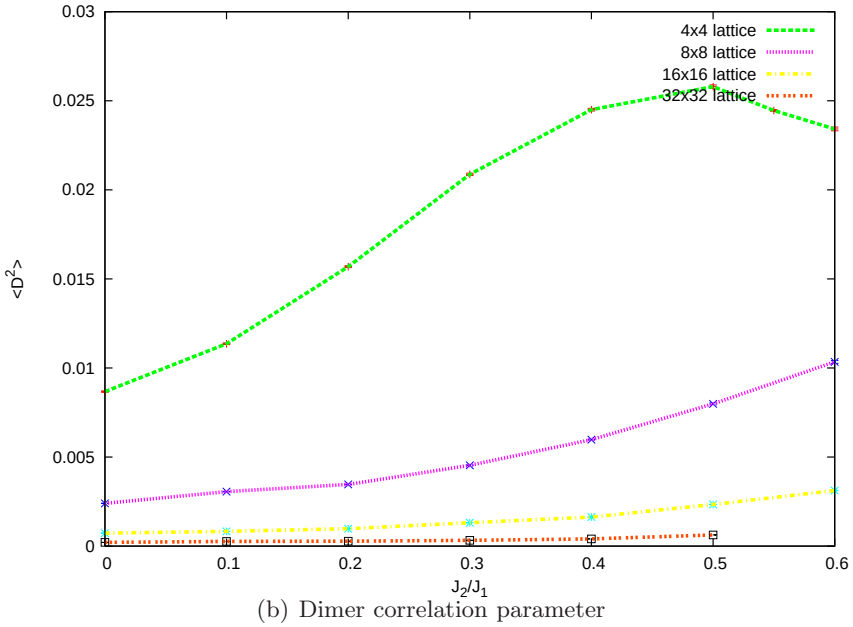

(b) Dimer correlation parameter

Figure 3.18: Symmetry breaking calculation results for 4×4, 8×8, 16×16 and 32×32 checkerboard AB pattern bond basis.

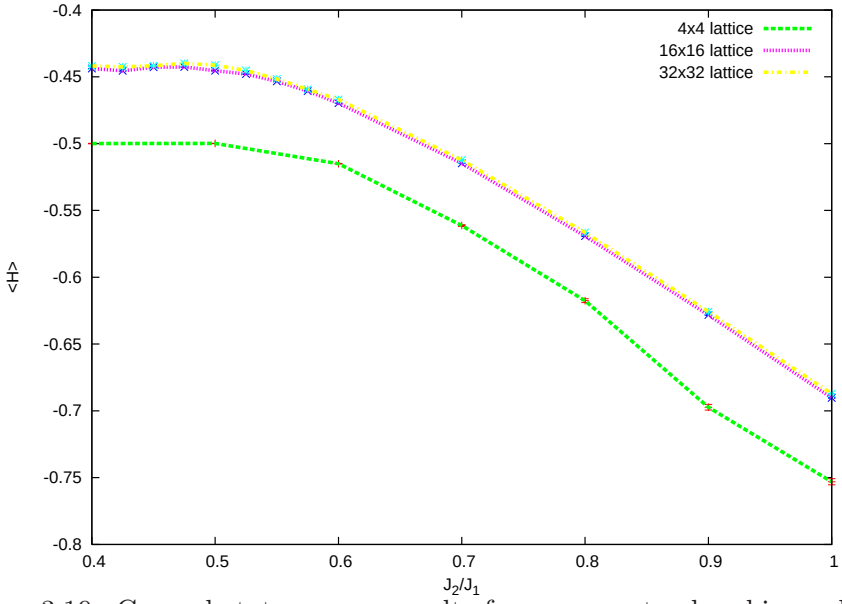

Figure 3.19: Ground state energy results from symmetry breaking calculation on 4×4, 16×16 and 32×32 collinear AB pattern bond basis.

3.3 Examining bond-bond correlation

In previous calculation, we took the trial wavefunction to be a product of independent bond amplitudes. It is proposed that the RVB variational trial wavefunction might be improved by considering some small symmetry breaking terms [Capriotti et al. (2001)] and the most direct approach is to add small correction terms concerning the correlation between bonds. As a result, more ordered bond configurations such as plaquette or columnar bond patterns will be favoured. A correction term $g_{ijkl} = g(\theta)$ can be applied to the original trial wave function. In this correction term, (i, j) and (k, l) are two neighbouring singlet bonds that form a group. θ is the angle between the bond (i, j) and (k, l). For example, we can choose the form $g(\theta) = 1 + a \cdot \cos^2(\theta)$ where $a \in [0, 1)$. When $a = 0$ the trial wave function reduces to its original form but $a \neq 0$ favours bond alignment. We can

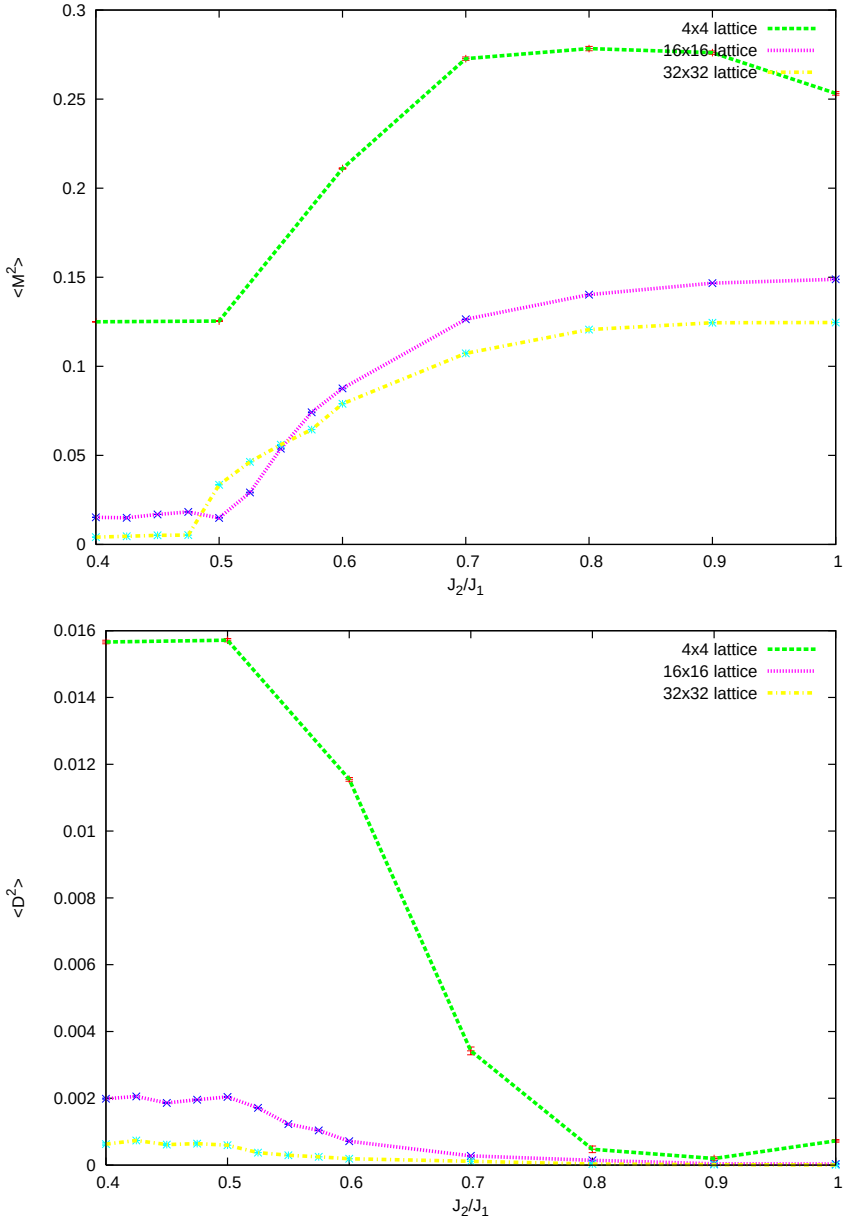

Figure 3.20: Symmetry breaking calculation results for 4×4, 16×16, 32×32 collinear AB pattern bond basis.

examine how the variational parameter a effects our system. The calculations are done with different values of a on a 4×4 lattice. The power-law exponent p increases so the bond configurations will become more short-ranged and gradually diminish the long-range magnetic order. With a increasing, more ordered alignment between bonds can be formed and the system becomes less magnetized (see Fig. 3.22).

The *group configuration* is also introduced by this correction term. Every two singlet bonds form a group and the update scheme is modified accordingly. In the original update scheme, the weight ratio between the old and new configuration only depends on the amplitudes of bonds.

With the group configuration taken into account, the update scheme is also extended to consider the group update. Each update step now involves two groups, i.e. four bonds. The group update scheme is shown as following,

1. Select two diagonal sites at random from a uniform distribution.
2. Check whether the two sites belong to the same group. If yes, skip to step 4.
3. Perform basic Metropolis updates for the two bonds, i.e. swap the bond ends for the two sites, which is accepted with a probability $P = \frac{h_{12}h_{36}h_{54}h_{78}}{h_{12}h_{34}h_{56}h_{78}} \cdot \frac{g_A+g_B+g_C}{g_A}$. Where h is the bond amplitude and g is the correction term for each group configuration.
4. Regroup to any of the possible combinations g_A, g_B, g_C with corresponding probability $P_x = \frac{g_x}{g_A+g_B+g_C}$.

The acceptance rate is sufficiently large to maintain the ergodicity for Monte Carlo calculations. The fluctuation in measurements (see Fig. 3.21(a),3.21(b)) shows that the group update scheme works properly without being stuck in certain bond configurations.

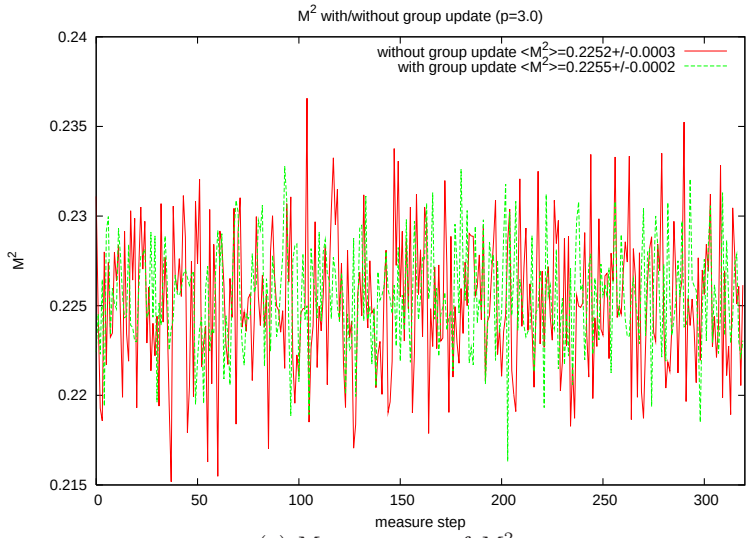

(a) Measurement of M^2

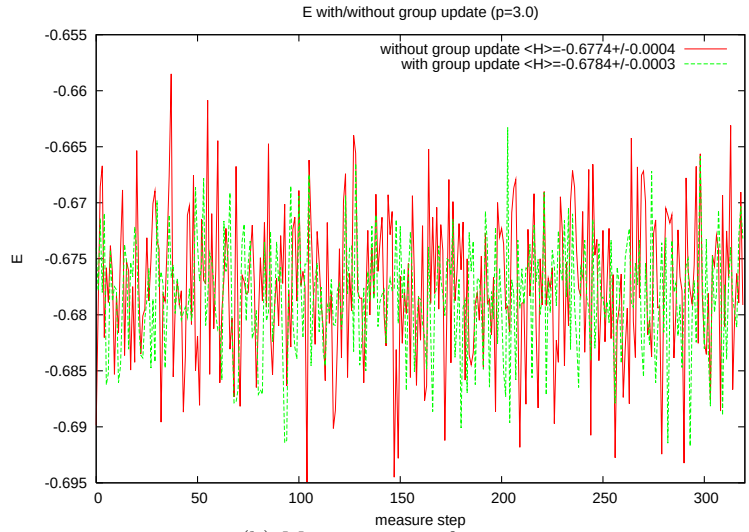

(b) Measurement of energy

Figure 3.21: M^2 and energy measured in each step with or without group update. Fluctuation in measurements shows the group update scheme works properly without being stuck in certain bond configurations.

The $g_{ijkl} = 1 + a \cdot \cos^2(\theta)$ is straightforward. However it may lead to uncontrollably large groups, which denotes a group formed by two far-apart bonds. The g term is expected to introduce parallel aligned bond configuration so that a small angle between neighbouring bonds is favored. As the formation of groups is uncontrolled, the actual effect of g can be that a small angle between both neighbor and far apart bonds is favored, and thus the overall configuration can not reach the highly oriented configuration as expected.

It is thus possible to reweight the formation of groups: when a new group is formed, the separation between two member bonds should also be taken into consideration. The g term can be modified to $g_{ijkl} = g(\theta) \cdot |\mathbf{r_i} - \mathbf{r_k}|^{-z} |\mathbf{r_j} - \mathbf{r_l}|^{-z}$. The site i and k are from different bonds and sublattices, l_{ik} is the distance between the two sites, z is the power law exponent. With a non-zero value of z, the groups tend to form between neighbouring bonds and an ordered bond pattern tend to be formed locally. When $z = 0$, g will return to the original form. This power law form is similar to the products of bond amplitudes in the original trial wave function and able to limit the groups to involve neighbour bonds. The trial wavefunction with correlation term however did not show any obvious improvements in the energy curve, instead the energy keeps increasing with frustration.

In our work we have presented how these descriptions of the phase fit the physics picture of the ground states in the strongly frustrated region. However, our system does have the possibility to exhibit some other phases. One question is whether it is capable of showing a hexatic phase, which appears, for example, in two-dimensional systems of hard discs. The discs behave as a gas of particles at low densities and approach close packing and form a solid at very high densities. An intermediate state might be found at moderately high densities in which the system has not yet solidified, i.e. has no long-range positional order (translational symmetry breaking).

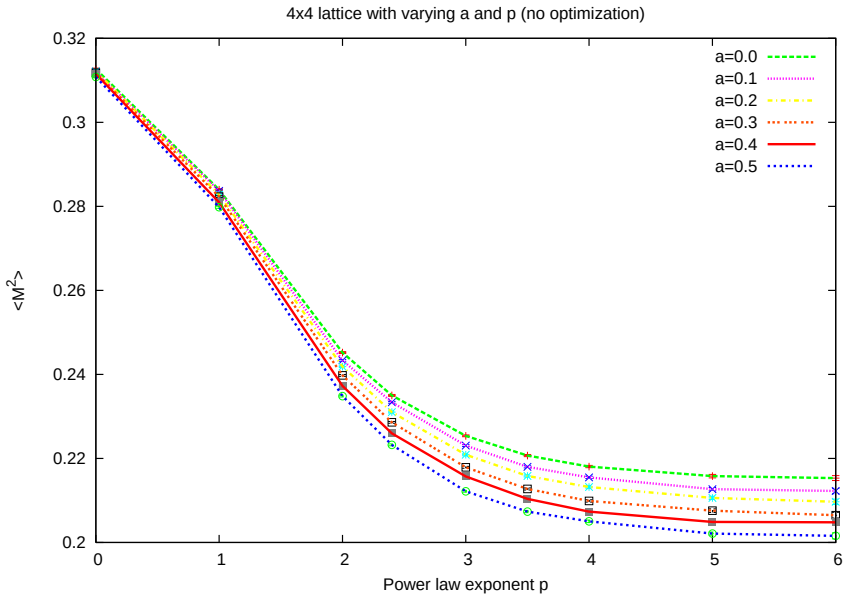

Figure 3.22: We examine how the variational parameter a affects the staggered magnetization by varying the value of a.

But over short distances around each particle, the system is beginning to develop the six-fold rotational symmetry breaking that is related to close packing. Therefore the rotational and translational symmetries can break in two distinct steps. When questioning whether something similar could happen in our case as short range dimers are packed onto the square lattice, the analogy to hexatic phase does not quite fit in our system. In the disc example, the system starts off with the full continuous rotational symmetry of free space and this comes into conflict with the six-fold symmetry preferred by close-packing. On the other hand, in our system, we start from a lattice, and the discrete symmetries of the lattice are identical to those of the packed dimers, and there is no competition.

It might be more relevant to compare our case to liquid crystal systems, where nematic and smectic phases can exist. The nematic phase can possibly emerge

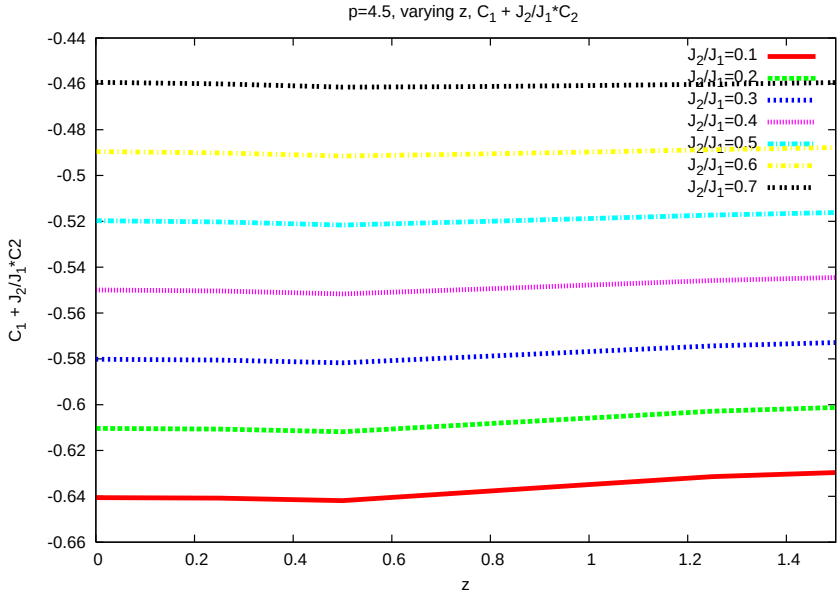

Figure 3.23: We fix the power-law exponent p and do variational calculation with z and obtain C_1 and C_2 results. We plot different linear combinations of C_1 and C_2 trying to obtain a minimum $\langle H \rangle = C_1 + J_2/J_1 \cdot C_2$. However the results show that there is not any minimum $\langle H \rangle$ for large J_2/J_1 value.

when the state has not solidified as a valence bond crystal but the bonds are more likely to be x-aligned rather than y-aligned. This could happen in our unbiased optimization scheme where the bond amplitudes take the form $h(|x|, |y|)$, however we did not find such a state in the actual calculation results.

CHAPTER 4

Conclusions

Our work focuses on studying the ground state of the Heisenberg model on the square lattice when a frustrating interaction is introduced. Novel quantum phases may exist due to frustration. Several possible descriptions of the ground state in the intermediate phase have been proposed: a valence bond crystal with columnar or plaquette order, or a spin liquid state, which is a purely quantum phase without any symmetry breaking or long range order. We take advantage of various numerical or analytical techniques to explore the possible descriptions of the ground state.

The ground state exhibits a semiclassical Néel order near $J_2/J_1 = 0$ and collinear magnetic order when J_2/J_1 is large. Accordingly we perform the calculations from both sides: using a bond basis adapted for checkerboard magnetic order or collinear magnetic order, respectively.

We start by examining the performance of the L.D.A. trial wavefunction on the frustrated Heisenberg model. The L.D.A. trial wavefunction begins to fail near $J_2/J_1 = 0.4$; the energy results on 4×4 lattice show growing discrepancy with exact diagonalization results, which implies some new form of trial wavefunction is needed to capture the correct physics.

Then we add more degrees of freedom to the L.D.A. trial wavefunction by reducing its full symmetry. The unbiased optimization is applied to the set of bond amplitudes. Energy and other order parameters are measured after the convergence is reached. We approach the intermediate phase region from both sides: small J_2/J_1 and large J_2/J_1. For the former we calculate with the checkerboard AB pattern bond basis and the latter we calculate with the collinear AB pattern. The result, especially the bond distribution, shows the amplitudes gradually become long-ranged along the main axis rather than simply showing algebraic decay in the L.D.A. trial wavefunction. Certain bond amplitudes quickly evolve to zero, which also indicates that they may be negative in the actual bond distribution but this can not be achieved in the unbiased calculation that only allows positive bond weights. The measurement of staggered magnetization on both sides $\mathbf{M}^2(\pi,\pi)$ and $\mathbf{M}^2(\pi,0)$ is gradually killed in the intermediate phase region. And the dimer correlation parameter $\mathbf{D}^2$ appears to increase in this region but as the lattice size growing it gradually scales to zero, which shows it may not survive in the thermodynamic limit.

We also apply a mean-field-like technique to make predictions of the bond amplitudes. A master equation is proposed to determine the form of the bond amplitude distribution. Unlike the bond amplitudes obtained from the unbiased optimization, the master equation allows that the bond amplitudes can evolve to both positive and negative value. In the master equation results, we confirm that the prediction in the unbiased optimization scheme that certain bond amplitudes have negative values. Also consistent with the unbiased optimization scheme, the bond amplitudes obtained from the master equation also exhibit 1D-like behaviour; becoming long-ranged along the main axis, which can be described as C_4 symmetry.

To examine whether the spin liquid could be a good description of the ground state in the intermediate phase region, we also perform short bond spin liquid Monte

Carlo calculations. All bonds are limited to nearest neighbour and long bonds are avoided to exclude any long range magnetic order. This kind of setup however brings problems in our previous update scheme. To solve this problem we adopted the Worm algorithm. The short bond spin liquid calculation results however have higher energy than the ground state on small lattice 4×4. The energy discrepancy is actually rather low near $J_2/J_1 = 0.4$ and 0.6 points, which may indicate that certain phase transitions happen around these points. More calculations are performed on larger lattice $8 \times 8, 16 \times 16, 32 \times 32$ and the energy results have larger discrepancy. Thus this spin liquid state may not act a true description of the ground state yet it still provides an upper bound for the ground state energy.

A symmetry-breaking calculation is performed to examine whether the columnar or plaquette valence bond crystal states have significantly lower energy. In the VMC calculation, all NN bonds are given full degrees of freedom so that the bond configuration can have spontaneous translational and/or rotational symmetry breaking. However the calculations on both sides show no obvious bond pattern with symmetry breaking. The bond amplitudes tend to form a uniform distribution with slight statistical fluctuation due to the stochastic optimization scheme. The symmetry-breaking calculation actually shows energy and order parameter results highly consistent with the unbiased optimization calculation, which indicates that the symmetry-breaking picture may not be real.

At last we try to consider the bond-bond correlation in the trial wavefunction. A correction term between bonds with alignment preference is added as in conjunction with additional variational parameters. However this new form of trial wavefunction proved to be unable to effectively lower the energy.

In our work we found no supporting evidence for the symmetry breaking or spin liquid description of the ground states in the intermediate phase region. Instead

the interesting behaviour of the bond amplitude distribution implies that some 1D description of the ground state is also possible.

Bibliography

Anderson, P. W. "Resonating valence bonds: A new kind of insulator." *Mater. Res. Bull.* 8 (1973): 153.

Anderson, P. W. "The Resonating Valence Bond State in La_2CuO_4 and Superconductivity." *Science* 235 (1987): 1196.

Balents, L. "Spin liquids in frustrated magnets." *Nature* 464 (03 2010): 199.

Beach, K. S. D. "Master equation approach to computing RVB bond amplitudes." *Phys. Rev. B* 79 (2009): 224431.

Beach, K. S. D. and A. W. Sandvik. "Some formal results for the valence bond basis." *Nucl. Phys. B* 750 (2006): 142.

Bishop, R. F., D. J. J. Farnell, and J. B. Parkinson. "Phase transitions in the spin-half $J_1 - J_2$ model." *Phys. Rev. B* 58 (1998): 6394.

Capriotti, L., F. Becca, A. Parola, and S. Sorella. "Resonating Valence Bond Wave Functions for Strongly Frustrated Spin Systems." *Phys. Rev. Lett.* 87 (2001): 097201.

Capriotti, L., F. Becca, A. Parola, and S. Sorella. "Suppression of dimer correlations

in the two-dimensional J_1-J_2 Heisenberg model: An exact diagonalization study." *Phys. Rev. B* 67 (2003): 212402.

Capriotti, L. and S. Sorella. "Spontaneous Plaquette Dimerization in the $J_1 - J_2$ Heisenberg Model." *Phys. Rev. Lett.* 84 (2000): 3173.

Dagotto, E. and A. Moreo. "Phase diagram of the frustrated spin-1/2 Heisenberg antiferromagnet in 2 dimensions." *Phys. Rev. Lett.* 63 (1989): 2148.

Fazekas, P. and P. W. Anderson. "On the ground state properties of the anisotropic triangular antiferromagnet." *Philos. Mag.* 30 (1974): 423.

Liang, S., B. Douçot, and P. W. Anderson. "Some New Variational Resonating-Valence-Bond-Type Wave Functions for the Spin-1/2 Antiferromagnetic Heisenberg Model on a Square Lattice." *Phys. Rev. Lett.* 61 (1988): 365.

Lieb, E., T. Schultz, and D. Mattis. "Two soluble models of an antiferromagnetic chain." *Ann. of Phys. (N.Y.)* 16 (1961): 407.

Lou, J. and A. W. Sandvik. "Variational ground states of two-dimensional antiferromagnets in the valence bond basis." *Phys. Rev. B* 76 (2007): 104432.

Marshall, W. "Antiferromagnetism." *Proc. Roy. Soc. A* 232 (1955): 48.

Richter, J. and J. Schulenburg. "The spin-1/2 $J_1 J_2$ Heisenberg antiferromagnet on the square lattice: Exact diagonalization for $N = 40$ spins." *Eur. Phys. J. B* 73 (2010): 117.

Richter, J., J. Schulenburg, A. Honecker, and D. Schmalfuß. "Absence of magnetic order for the spin-half Heisenberg antiferromagnet on the star lattice." *Phys. Rev. B* 70 (2004): 174454.

Sandvik, A. W. "Ground State Projection of Quantum Spin Systems in the Valence-Bond Basis." *Phys. Rev. Lett.* 95 (2005): 207203.

Sandvik, A. W. "Computational Studies of Quantum Spin Systems." *AIP Conf. Proc.* 135 (2010): 1297.

Schulz, H. J., T.A.L. Ziman, and D. Poilblanc. "Magnetic Order and Disorder in the Frustrated Quantum Heisenberg Antiferromagnet in Two Dimensions." *J. Phys. I France* 6 (1996): 675.

Sushkov, O. P., J. Oitmaa, and W. Zheng. "Quantum phase transitions in the two-dimensional $J_1 - J_2$ model." *Phys. Rev. B* 63 (2001): 104420.

Syljuåsen, O. F. and A. W. Sandvik. "Quantum Monte Carlo with directed loops." *Phys. Rev. E* 66 (2002): 046701.

Zhitomirsky, M. E. and K. Ueda. "Valence-bond crystal phase of a frustrated spin-1/2 square-lattice antiferromagnet." *Phys. Rev. B* 54 (1996): 9007.

APPENDIX A

Appendix

A.1 Rewrite the Total Energy into the Form of Weights

$$
\begin{aligned}
|\psi\rangle &= \sum_{\sigma} \psi(\sigma)|\sigma\rangle \\
\frac{\langle\psi|\hat{O}|\psi\rangle}{\langle\psi|\psi\rangle} &= \frac{\sum_{\sigma,\sigma'} \psi(\sigma)^*\psi(\sigma')\langle\sigma|\hat{O}|\sigma'\rangle}{\sum_{\sigma,\sigma'} \psi(\sigma)^*\psi(\sigma')\langle\sigma|\sigma'\rangle} \\
&= \frac{\sum_{\sigma,\sigma'} \psi(\sigma)^*\psi(\sigma')\frac{\langle\sigma|\hat{O}|\sigma'\rangle}{\langle\sigma|\sigma'\rangle}}{\sum_{\sigma,\sigma'} \psi(\sigma)^*\psi(\sigma')\langle\sigma|\sigma'\rangle} \\
&\equiv \frac{\sum_L W(\mathcal{L})O(\mathcal{L})}{\sum_L W(\mathcal{L})} \\
\mathcal{L} &= (\sigma,\sigma') \\
W(\mathcal{L}) &= \psi(\sigma)^*\psi(\sigma')\langle\sigma|\sigma'\rangle \\
O(\mathcal{L}) &= \frac{\langle\sigma|\hat{O}|\sigma'\rangle}{\langle\sigma|\sigma'\rangle}
\end{aligned}
$$

A.2 Derivation of the Optimization Formula

$$
\begin{aligned}
\frac{\partial\langle H\rangle}{\partial h(l)} &= \frac{\sum_{\mathcal{L}} \frac{\partial W}{\partial h(l)} E(\mathcal{L})}{\sum_{\mathcal{L}} W(\mathcal{L})} - \frac{\sum_{\mathcal{L}} W(\mathcal{L})E(\mathcal{L})}{(\sum_{\mathcal{L}} W(\mathcal{L}))^2} \sum_{\mathcal{L}} \frac{\partial W}{\partial h(l)} \\
\frac{\partial W}{\partial h(l)} &= \frac{\partial}{\partial h(l)} \prod_{l'} h(l')^{n(l')} \\
&= \prod_{l \neq l'} h(l')^{n(l')} \cdot n(l) h(l)^{n(l)-1} \\
&= \frac{n(l)}{h(l)} W\mathcal{L} \\
&\quad Thus \\
\frac{\partial\langle H\rangle}{\partial h(l)} &= \frac{1}{h(l)}[\langle n(l)H\rangle - \langle n(l)\rangle\langle H\rangle]
\end{aligned}
$$